UNIVERSITY OF TARTU

FACULTY OF SCIENCE AND TECHNOLOGY

Līga Britāla

DIELECTRIC METASURFACES FOR CO_2 GAS SENSING

Master's thesis

Materials Science and Technology

30 ECTS

Supervisor: Dr. Glen Kelp

Tartu 2021

ANNOTATION

Dielectric metasurfaces for CO_2 gas sensing. Britala L., supervisor Dr. phys., Kelp G.. Master's thesis, 49 pages, 19 figures, 2 tables, 53 references, 8 appendices. In English.

Dielectric metasurfaces exhibit many properties that could improve the detection capabilities of a gas sensor, such as high quality factor resonances, and high field enhancement, providing sensitivity to changes in refractive index or specific molecular absorption lines of gases. Incorporating infrared (IR) active metasurfaces in high precision CO_2 sensors could enable a sensitive, small, convenient, fast responding, and cost-efficient device.

In this work the aptitude for CO_2 sensing of four dielectric metasurface designs is explored and verified by conducting numerical studies. Numerical simulations give justification for the experimental work which would probe the IR light absorption of metasurfaces in transmission mode over various mid-IR CO_2 molecular absorption wavelengths. Suitability of all types of metasurfaces for CO_2 gas sensing is discussed.

Keywords: metasurfaces, CO_2, gas sensing, IR, optical resonance, field enhancement

CERCS classification: P200 Electromagnetism, optics, acoustics

ANNOTATSIOON

Dielektrilised metapinnad CO_2 gaasi tuvastamiseks. Britala L., juhendaja Dr. Kelp G. Magistritöö, 49 lehekülge, 19 joonist, 2 tabelit, 53 viidet, 8 lisa. Inglise keeles.

Dielektilistel metapindadel on mitmeid omadusi, mis võimaldaksid nende kasutamist täpsete gaasisensoritena, sealhulgas suure hüveteguriga resonantsid ja tugevad lokaalsed elektriväljad, pakkudes tundlikkust murdumisnäitaja või gaaside molekulaarsete neeldumisjoonte muutuste suhtes. Infrapuna aktiivsete metapindade kasutamine suure täpsusega CO_2 sensorites oleks aluseks tundlike, väikeste, mugavate, kiire reaktsiooniajaga ja kuluefektiivsete seadmete loomisel.

Käesolev töö uurib nelja erineva dielektrilise metapinna geomeetrilise konfiguratsiooni sobivust CO_2 sensorrakenduseks kasutades numbrilisi uurimismeetodeid. Antud töös läbi viidud numbrilised simulatsioonid loovad aluse eksperimentaalseks tööks, kus mõõdetaks infrapuna valguse neeldumist metapinnas läbivusrežiimis CO_2 neeldumisjoontel keskinfrapunases spektripiirkonnas. Töös käsitletakse kõigi valitud metapindade sobivust CO_2 gaasi detekteerimiseks.

Märksonad: metapinnad, CO_2, gaasisensorid, infrapuna, optilised resonantsid, väljavõimendus

CERCS klassifikaator: P200 Elektromagnetism, optika, akustika

TABLE OF CONTENTS

Abbreviations

2D – two-dimensional

BAW – bulk acoustic wave

CMOS – complementary metal oxide semiconductor

EBL – electron beam lithography

EM – electromagnetic

FE – field enhancement

IR – infrared

LOD – limit of detection

MOS – metal oxide semiconductor

NDIR – non-dispersive infrared

PML – perfectly matched layer

Q – quality factor

Ra – resistance of the MOS sensor in reference gas (usually air)

Rg – resistance of the MOS sensor in analyte gas

SAW – surface acoustic wave

SOI – silicon on insulator

1 Introduction

Despite extensive research and developments in the CO_2 gas sensor field, the task of creating a small, sensitive, cost-efficient, selective, and quickly responding detector remains a challenge. There are several methods of detecting CO_2 gas, such as electrochemical, metal oxide semiconductor (MOS), calorimetric, optical, and others, that each have their advantages and disadvantages. For example, MOS detectors can have very high sensitivities, however, their drawbacks include high working temperatures and bulky size, which is also a characteristic of electrochemical detectors. For gas sensing applications usually the most reliable method has proven to be optical detection, for CO_2 specifically – the non-dispersive infrared (NDIR) technique.

The method for CO_2 sensing explored in this work is based on IR spectroscopy, which is an optical method that utilizes the asymmetrical C-O double bond stretching in the CO_2 molecule at around 4.3 μm which creates an absorption band in this frequency region. When sensing with metasurfaces, high-Q spectral features of metasurfaces are tuned to coincide with these narrow CO_2 molecular absorptions at 4.3 μm to achieve high sensitivity and specificity through interaction of gas molecule vibrational modes with metasurface resonances while exciting the sensor surface with IR radiation.

In terms of business value, this work is very promising. The compound annual growth rate for the gas sensor market, value of which in 2019 was 1.5 billion USD, between 2020 and 2026 is estimated to be 5%. Out of the total gas sensor market the revenue share held by the CO_2 gas sensor market is a substantial 20% and is expected to grow around 4% by 2026[1]. Considering the COVID-19 related increase in the need for air quality monitoring systems, the market share may increase even more rapidly as the demand for CO_2 sensors grows.

The aim of this work is to provide theoretical justification for the use of metasurfaces in CO_2 gas sensing which could potentially provide a way to overcome drawbacks of currently available CO_2 sensors, such as low sensitivity, slow response time, bulky size, and high cost.

2 Theoretical Background

2.1 Gas sensing

Gas sensing is the identification and quantification of gases. Most often it includes measuring the concentration of a specific gas to characterize certain processes or environments.

Gas sensing has been growing and developing rapidly over the past few decades, as the concentration of various gases in different environments has proven to be an accurate tool for describing and predicting the state of a myriad of processes and entities. Especially in recent years, as it has been integrated in smart technology for such applications as meat freshness evaluation[2], detection of fresh vegetables freezing time[3], oestrus determination to indicate the fertile period in female cattle[4], identify anomalies in ozone measurements[5], pollutant gas detection[6], disease diagnosis from human breath[7], and a variety of other applications in industry and research.

There are many technologies employed in different gas sensors, each with their advantages and disadvantages. The reason why gas sensing is still being researched widely and new smart sensing methods are being developed is due to challenges which are present specifically in gas sensing, because gas activity is greatly dependent on the temperature and humidity of the surrounding environment, which directly affects the accuracy of gas sensors.

2.2 Gas sensors

Currently available gas sensors are based on a vast variety of technologies. Among them are metal oxide semiconductor sensors, electrochemical sensors, calorimetric sensors, capacitance-based gas sensors, acoustic gas sensors, and optical gas sensors. There are many parameters which are commonly used to describe the performance quality of gas sensors and each type of gas sensor excels in some categories and exhibits flaws in others.

Among the characteristics used to describe gas sensors are **sensitivity**, which is the change in the measured signal based on the change in analyte (gas) concentration, **selectivity**, which describes how well a sensor can distinguish separate gases in a mixture of many, **stability**, which defines the reproducibility of sensor measurements and how well the sensitivity, selectivity, response, and recovery times are retained, **detection limit (LOD)**, often mistaken for sensitivity, is the lowest analyte concentration which can be detected under specific conditions, **dynamic range**, which describes the range of gas concentration which can be reliably detected (lower detection limit to highest limiting concentration), **linearity**, which

characterizes how much the calibration graph deviates from an ideal straight line, **resolution**, describing the minimum measurement unit which is displayed by the instrument, **response time**, which is the time it takes for a gas sensor to respond and register a step change in analyte concentration, **recovery time**, describing how long it takes for the sensor signal to return to its initial value after a step concentration change back to zero, **working temperature**, which is usually the temperature at which the sensor's sensitivity is maximum, **hysteresis**, which is the difference in the signal value when the value is approached with an increasing or decreasing concentration range, and **life cycle**, which describes how long the sensor will continuously operate reliably[8].

The sensor explored in this work is based on the optical method of gas sensing, however, a brief description of other common sensor types, their applications, advantages and disadvantages, and brief evaluation of the quality of some parameters are given.

2.2.1 Metal oxide semiconductor (MOS) gas sensors

MOS gas sensors are most widely used in food and beverage industry and indoor and outdoor gas level monitoring. They operate by sensing the variation in the electrical properties of a gas. In general, when the semiconductor material is heated to high temperatures in air, the electrons in the material become attracted to the oxygen atoms in the surrounding air. Oxygen atoms are then adsorbed on the surface of the sensing material and inhibit the electric current flowing through it. If the atmosphere surrounding the sensor contains reducing gases, they react with the oxygen molecules on the semiconductor surface, reducing the density of the adsorbed oxygen molecules and facilitating the electric current flow through the semiconductor material. For oxidizing gas detection, the mechanism includes competitive adsorption on the MO surface of the oxidizing gas molecules. The mechanism and response slightly varies depending on the type of semiconductor used and the analyte[9].

The operating temperature of MOS gas sensors is relatively high, more than 400°C, making it quite unsuitable for everyday gas concentration monitoring at home or hand-held devices. The high operating temperature, however, can also be an advantage, depending on the target application.

Sensitivity of MOS sensors is good, it can be described as the ratio (Ra/Rg) of the resistance of the sensor in the reference gas, usually air (Ra) to the resistance of the sensor in the analyte gas (Rg) for oxidizing gases and vice versa (Rg/Ra) for reducing gases[10]. It greatly depends on the grain size, microstructure (which influences surface area), and dopants added to the metal

oxide[11]. Additionally, the sensitivity of a MOS sensor is affected by presence of humidity in the surrounding environment[12].

The reliable working range of MOS detectors typically reported in literature for CO_2 gas sensing covers the range of 2000-10000 ppm, being most responsive in the 2000-5000 ppm range[13].

2.2.2 Electrochemical gas sensors

This type of gas sensor utilizes the electrochemical cell for sensing purposes. The simple cell includes two electrodes (working and counter electrode) connected by an external wire, which is electron-conducting, and by an electrolyte, which is ion conducting. The measured parameter in this system is the electrical current flowing through the wire connecting the electrodes, which changes linearly with changing analyte gas concentration.

When an analyte gas, such as CO, comes in contact with the working electrode in the presence of water molecules (water vapour in air), it becomes oxidized via the following chemical reaction:

$$CO + H_2O \rightarrow CO_2 + 2H^+ + 2e^- \quad (1)$$

The H^+ ions diffuse through the electrolyte to the counter electrode where they react with the oxygen in the air to form water:

$$2H^+ + 1/2O_2 + 2e^- \rightarrow H_2O \quad (2)$$

And the two electrons from the first reaction flow through the external wiring to participate in the reaction at the counter electrode.

Among the applications of the electrochemical type sensor are air monitoring, medical, security, and industrial applications.

This sensor is attractive due to its low production cost, power efficiency, wide range of operating temperatures, and sensitivity to a wide variety of different gases, however, it's disadvantages include limited sensitivity and large size[14]. The detection range of electrochemical sensors is 0–1000 ppm, adjustable[14].

2.2.3 Calorimetric (catalytic type) gas sensors

Calorimetric gas sensors work by detecting the heat evolved by combustible gases on the heated sensor surface. The heat from the exothermic reaction of a gas combusting on the metal surface slightly raises the temperature, in turn raising the resistance of the sensor material (metal). This resistance change is then detected via external wiring.

This type of sensor was developed already in the 1950's for detecting methane in coal mines. Then it was a Pt coil which was heated to 900°-1000°C[15]. Nowadays this sensor is still mainly used in areas where combustible gases are detected for safety. These include leak detection, combustible gas detection in mining, oil and gas production, sewer gas and landfill gas.
The detection range for this type of sensor is 200–1000 ppm for both H_2 and CH_4[16], however, it may differ for other combustible gases.
These sensors are typically small, portable, with low production cost and power consumption, and long lifetime. However, this sensor needs to be frequently recalibrated and the catalyst for the combustion reaction is susceptible to poisoning by other gases. Additionally, the combustible gases can only be detected in the presence of oxygen, for the combustion reactions to take place[15].

2.2.4 Capacitance-based gas sensors

Capacitance based gas sensors also mainly employ metal oxides like the MOS gas sensor, however, here the gas concentration is determined by evaluating the change in capacitance.
Capacitance is calculated as

$$C = \varepsilon_0 \varepsilon_r A/d \quad (3)$$

where ε_0 is the permittivity in vacuum (dielectric constant), ε_r is the relative permittivity, A is the electrode area, and d is the thickness of the dielectric layer (the distance between electrodes). A sensor which detects change in capacitance detects change in one of the parameters which express it[17].
Advantages of capacitive type sensors include simple structure, possibility for miniaturization, and increased selectivity due to changes in capacitance being highly selective for different physical phenomena. However, capacitance depends on temperature, therefore temperature monitoring along gas sensing measurements would be necessary.
Lower LOD (for CO_2) for a capacitive type gas sensor which employs $CuOBaTiO_3$ is 100 ppm, however, it can be decreased to 50 ppm by adding Ag. The upper LOD, depending on the metal oxide used, can reach up to 200000 ppm[17].

2.2.5 Acoustic wave gas sensors

There exist a variety of acoustic wave sensors. The most frequently utilized types in gas sensing are bulk acoustic wave (BAW) and surface acoustic wave (SAW) sensors. The principle behind the SAW sensor is the detection via a piezoelectric component of how different gases change

the characteristics of a surface acoustic wave. A reference wave is also being generated, which does not come in contact with the analyte and serves as a point of reference for the measurement.

Acoustic type sensors can be used for environmental monitoring, chemical detection, automotive, and food and beverage industry.

The advantages of acoustic type sensors include response to nearly all gases, good sensitivity, short response time, small size, and low cost. One of the biggest disadvantages of this type of sensor is very bad signal to noise ratio.

The detection range is 100–400 MHz[14].

2.2.6 Optical gas sensors

Optical sensors can detect gas concentration based on a variety of optical phenomena, such as fluorescence, colour change (colorimetric), optical layer thickness change, light attenuation, and absorbance. In the most popular type of optical gas sensors for CO_2 measuring, the non-dispersive infrared (NDIR) sensors, the measured property by which the gas concentration is determined is IR light absorption by CO_2 gas at the vibrational frequency of around 4.3 µm. It is determined by detecting the decrease in transmitted light intensity through a layer of gas. Principles of CO_2 gas detection by the NDIR method are described in more detail in the section "2.4 CO_2 gas sensing".

In general, optical gas sensors are used in environmental monitoring and biomedical applications, largely due to being very non-destructive of the analyte and non-invasive. Other advantages include low power consumption, high sensitivity, selectivity, and rapid response. However, these sensors are affected by light interference and it can prove difficult to implement them in smart technology such as an electronic nose[14]. Additionally, low cost and light weight of NDIR CO_2 detectors has not yet been successfully achieved without compromising their accuracy and sensitivity[18].

The detection range of optical sensors depends on what optical characteristic is being measured. For NDIR gas detectors the short term limit of detection as low as 1 ppm has even been achieved up to upper limit of detection of 200000 ppm of CO_2 gas[19]. However, these parameters may vary depending on the underlying technology of the NDIR device.

The CO_2 sensing method explored in this work is based on the optical detection principles.

2.4 CO_2 gas

2.4.1 Physical properties

CO_2 is a binary compound which exists as a gas in standard conditions. It is odourless, colourless, having higher density than air, with a molar mass of 44.01 g/mol. It is a linear molecule with C as the central atom covalently double bonded to two O atoms on opposite sides (fig. 1), hence, the molecule is non-polar as the dipoles on the polar covalent bonds cancel each other out on opposite sides.

The electron configuration of CO_2 makes it relatively unreactive (see "2.4.2 Chemical properties"). The two covalent bonds between each O and the central C and the probability of electrons to exist in every place at any given instance ensures that all atoms in the molecule have 8 electrons in the outer electron shell (filled outer shell).

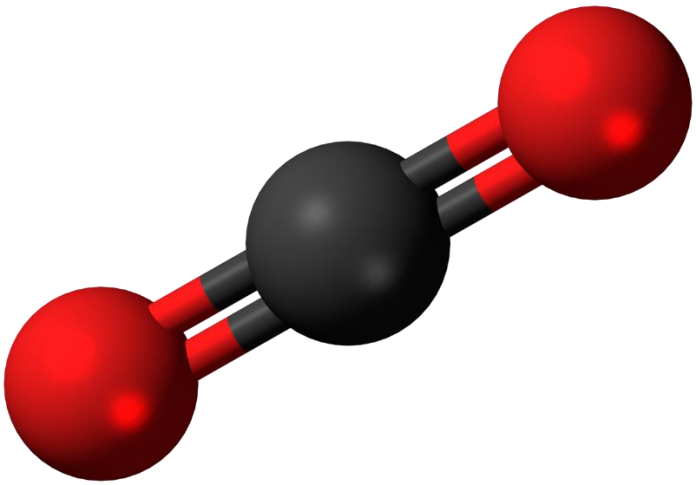

Figure 1. CO_2 molecule structural representation. The black atom in the middle is carbon; the red atoms on the sides are oxygen[20].

2.4.2 Chemical properties

CO_2 is an acidic oxide and reacts with basic substances such as NaOH to form salt and water.

$$CO_2 + 2NaOH \rightarrow Na_2CO_3 + H_2O \quad (4)$$

However, the number of spontaneous reactions with CO_2 is limited.

CO_2 is very slightly soluble in water – in a fully reversible reaction with water CO_2 forms carbonic acid.

$$CO_2 + H_2O \leftrightarrow H_2CO_3 \quad (5)$$

CO_2 is also considered an inert gas. This is a property usually associated with noble gases such as He, Ne, and Ar which exist as gases in their elemental form and possess very, very low reactivity. Another non-noble gas which is inert is N_2. All these different gases are inert

(possess low reactivity) due to having a filled outer electron shell and removing electrons from the shell requires large amount of energy, thus reactivity is hindered.

CO_2, as opposed to the noble gases, ensures the filled outer shells by sharing electrons in covalent bonds, which allows the electrons to move more freely in the molecule. Therefore, reactions with CO_2 may still occur, provided enough energy. For example, when carrying out tungsten inert gas welding in CO_2 gas atmosphere, CO_2 reacts with the metals, oxidizing them and making the connections more brittle[21].

2.4.3 Occurrence

CO_2 is one of the gases present in the Earth's atmosphere. It occurs in varying concentrations inside buildings and at different altitudes. The average atmospheric concentration is currently around 412 ppm[22].

It is relatively nontoxic, however certain concentrations of CO_2 can be lethal for humans and animals. The effect of different levels of CO_2 on human health is listed in table 1.

Table 1. Effect of different levels of CO_2 on human health[23].

Concentration, ppm	Effect on health
200 - 400	Normal concentration; no effect
400 – 1000	Typical concentration in spaces with good ventilation; no effect
1000 – 2000	Poor air in buildings; drowsiness
2000 – 5000	Stagnant, stuffy air; sleepiness, headaches, poor concentration, nausea
>5000	Exposure limit for daily workplace exposure; oxygen deprivation
>40000	Serious oxygen deprivation; brain damage, coma, death.

While at certain concentration levels CO_2 is toxic to humans, for plants increased levels of CO_2 have shown to result in increased crop yields and decreased water consumption[24], however, the leaves of plants also start thickening, and the CO2 sequestration becomes less efficient, decreasing the global carbon sink by 8 PgC/year, which is the amount of current annual fossil fuel emissions[25].

2.5 CO_2 gas sensing

Monitoring the CO_2 concentration in air and water on Earth is of crucial importance in ensuring equilibrium in consumption and emission of this greenhouse gas. Several methods for this

purpose have been developed, the most widely and reliably used being the NDIR gas sensors[19,26], electrochemical sensors[26] and metal oxide semiconductor-based CO_2 sensors[9,11,13,26]. The metal oxide semiconductor-based sensors have fast response to CO_2 level change and low detection limit, and electrochemical sensors have simple setup and require relatively low maintenance, however, both sensor type detection reliability is impaired by cross-responding to other atmospheric gases and water vapour[19]. In contrast, NDIR sensors are not affected by other gases and show great specificity[26]. In CO_2 detection, optical methods are shown to be most suitable[27].

Optical CO_2 detection (namely NDIR) is based on the absorption of IR light at the frequencies of molecular bond vibrations. For CO_2 there are 4 normal modes, of which 3 generate a dipole moment and are therefore IR active (produce a signal in the IR spectroscopic range)[28]. Of these 3, the preferred mode for sensing is the asymmetric bond stretching, generating a signal at around 4.3 μm (2359 cm^{-1}) – in the mid-IR region.

In IR sensors the difference between the intensity of light emitted from the source and the light detected after passing through a sample chamber is measured. In most optical sensors the attenuation of the IR light signal as it passes through low concentration of analyte is governed by the Beer-Lambert law

$$I(\lambda) = I_0(\lambda)e^{-\alpha(\lambda)cl} \tag{6}$$

which shows the relation of the detected optical intensity at wavelength λ I(λ) [W/m^2] to the emitted optical intensity at wavelength λ $I_0(\lambda)$ [W/m^2], the absorption coefficient of the gas α(λ) [L/gm], the concentration of the analyte gas c [g/L], and the length of the gas chamber (fig. 2) where light-gas interaction occurs l [m][29].

The Beer Lambert law can also be expressed in the form

$$A = \varepsilon cl \tag{7}$$

where absorbance A is calculated by multiplying the molar attenuation coefficient ε (also known as molar extinction coefficient, molar absorptivity, or molar absorption coefficient), attenuating species concentration c, and the path length for the light to travel through the attenuating species l (gas chamber length in fig. 2).

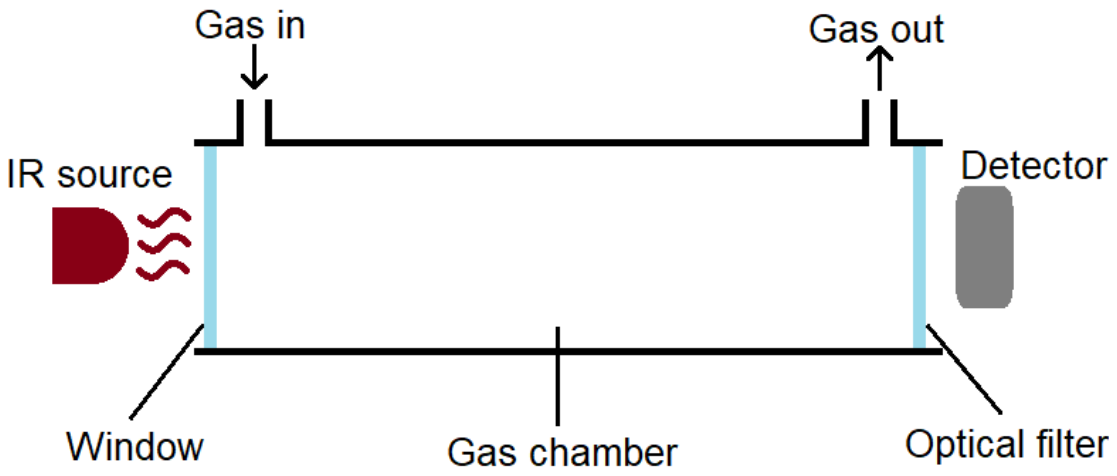

Figure 2. NDIR gas detector schematic representation.

The reason behind CO_2 being IR active and absorbing light of these frequencies is that the natural resonance frequency of the molecule matches the IR light frequency. The dipole moment in the molecule is dictated by the charge difference magnitude and the distance between the opposing charge centres. If the frequency at which the dipole moment fluctuates as the molecule vibrates matches the radiation frequency, the light is absorbed and consequently the amplitude of molecular vibration is altered[30].

2.6 Metasurfaces

Metasurfaces are the very thin analogues of metamaterials – periodic arrays of structures (unit cells) with specific geometry that can achieve unnatural properties, such as extraordinary electromagnetic or acoustic behaviour to manipulate electromagnetic and sound waves, respectively. Notably, negative refractive index n can be achieved[31], enabling wide-range wave manipulation. The unique properties of metamaterials give rise to several interesting and useful applications such as invisibility cloaking by light manipulation[32], sound insulation by absorbing acoustic waves[33], and antenna applications[34], to list a few. Metasurfaces possess the same ability, however their size in one dimension is significantly reduced (to sub-wavelength scale when considering the IR frequency region). Such thickness reduction essentially makes metasurfaces 2D materials.[35]

The nano-scale engineering and materials used in IR active metasurface fabrication enable high field enhancement inside the material or in its close vicinity and extremely sharp resonance features in transmission, reflection and/or emission spectra as the metasurface is excited with

IR radiation. Field enhancement is the increase in local electric field intensity. In molecule sensing with metasurfaces high values of field enhancement are desired for increased spectral feature interaction with molecular vibrations. Sharp spectral resonance features improve molecule sensing as well. When carrying out measurements at a certain frequency that corresponds to the resonance maximum or the steep slope of the resonance feature, upon changes in the surrounding environment (such as refractive index change[36–39] or molecular vibrations[40,41]) high modulation in the signal intensity will be generated, since in sharp features even slight deviations produce noticeable changes. Thus, having both, a strong field enhancement and sharp resonance features exhibited by the metasurface allows for high sensitivity and selectivity in sensing.

The metasurface unit cell geometries explored in this work are represented in section "3 Experimental Part". The dimensions of the structures are tuned so that they would exhibit a spectral resonance feature at a desired wavelength (4.3 μm for CO_2 gas detection). By matching the resonance feature to the CO_2 absorption wavelength, coupling between the metasurface resonance and CO_2 vibrational modes can be observed, causing the transmitted (or reflected) signal to change, which can then be employed in CO_2 gas sensing.

2.7 Metasurfaces in CO_2 gas sensing

CO_2 gas sensing with metasurfaces is based on IR absorption spectroscopy and utilizes the asymmetric bond stretching of the CO_2 molecule at around 4.3 μm. At this wavelength CO_2 exhibits an absorption maximum (or a transmission minimum) in the IR spectrum.

As IR light is shone on the system, the metasurface resonant modes are excited by the electric field of the EM radiation and create high field enhancement. Metasurface geometries can be tuned so that their resonant modes coincide with the vibrational resonances of the CO_2 molecules. If CO_2 is present in the vicinity of the metasurface, at around 4.3 μm the strongly enhanced electric field around the metasurface excites the CO_2 molecular vibrations which in turn modulate the transmitted or reflected signal. Interaction between the metasurface resonant mode at around 4.3 μm and CO_2 vibrational modes may cause shift in the resonance peak of the metasurface or other modulations in the spectrum, such as appearance of a Fano feature[42], that in turn induce a change in the signal intensity which can then be detected.

High field enhancement around the metasurface combined with a high-Q metasurface resonance peak is the key to high sensitivity CO_2 gas sensing, as described in section "2.5 Metasurfaces". This is because high field enhancement means enhanced light-matter

interactions and a sharp resonance peak means that even miniscule modulations in its position or shape caused by minute amounts of CO_2 would cause noticeable changes in the transmitted or reflected signal intensity.

Field enhancement (FE) is described as the ratio of the field strength squared ($|E|^2$) to the incident field strength squared ($|E_0|^2$):

$$FE = |E|^2/|E_0|^2 \quad (8)$$

And the quality factor Q of the resonance peaks can be calculated as the ratio of the resonance frequency (or wavelength λ_{res}) to the width of the peak at half height $\Delta(\lambda)_{h/2}$.

$$Q = \lambda_{res}/\Delta(\lambda)_{h/2} \quad (9)$$

The physical meaning of the Q factor is evaluating how strongly damped an oscillator is. The higher the Q factor, the longer the oscillator will retain its energy and the oscillations will thus die out more slowly. Essentially, a higher Q factor means lower damping and a more noticeable modulation in signal intensity in response to the presence of analyte.

The schematic representation of how metasurfaces could be incorporated in the gas sensing system is shown in figure 3. Broadband or laser IR source is used to excite the metasurface. CO_2 gas concentration in the vicinity of the metasurface is detected through the modulation of transmittance at CO_2 IR absorption wavelength (approx. 4.3 μm). For polarization sensitive metasurfaces, polarizer or both polarizer and analyzer are used.

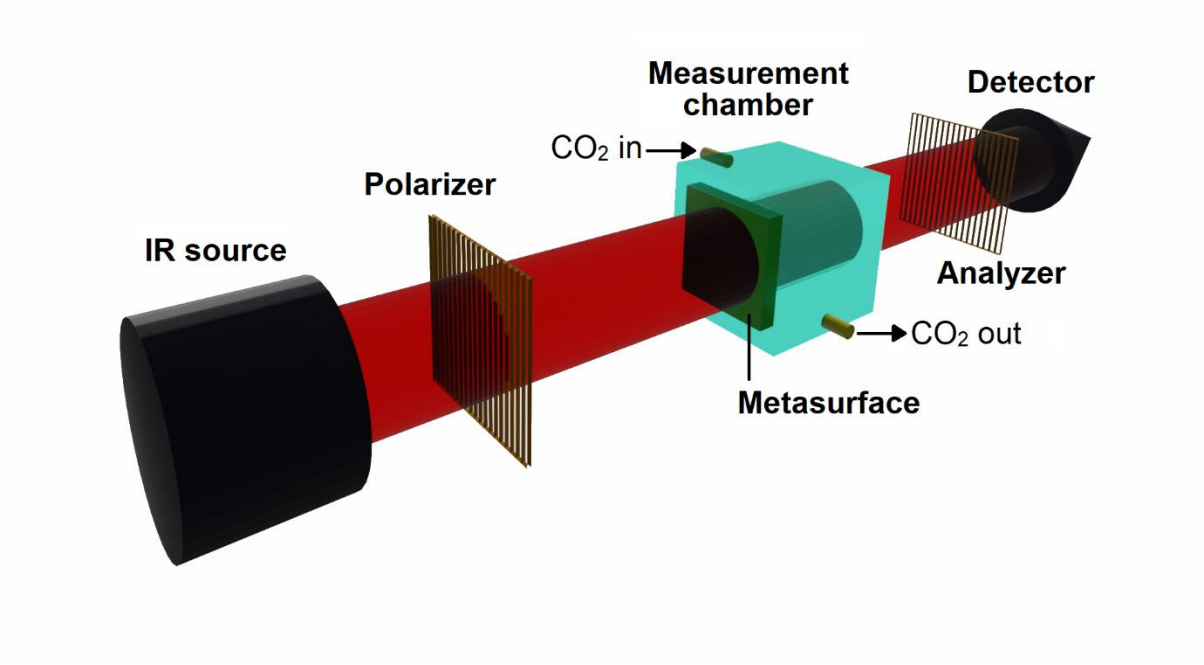

Figure 3. Schematic representation of a metasurface incorporated in an IR CO_2 sensing device.

2.8 Dielectric metasurfaces

At first glance the properties of dielectric metasurfaces do not seem very attractive with electromagnetic fields being localized mostly within the unit cell material and field enhancement being lower than for plasmonic (metallic) structures with similar configuration, meaning not much light-matter interaction enhancement occurs. However, to overcome the limitations of plasmonic metasurfaces, such as high radiative and resistive losses and resistive heating, investigation of their dielectric counterparts has gained great interest.

To tackle the obstacle of electromagnetic fields being confined dominantly within the dielectric metasurface material, it has been shown that introducing narrow gaps in dielectric nanoresonators provides a way for the fields to be localized outside of the structures[43] which would enable stronger light-matter interactions. Additionally, research has verified that introducing a symmetry-breaking element in the unit cell geometry[44] enables for additional dark resonant modes to be present and thus via coupling to the bright modes create sharp Fano resonant features which have exceptionally high Q factors. Having high Q factors is especially beneficial in gas sensing, particularly CO_2, where one of the main struggles with detectors currently available remains their cross-sensitivity to other gases.

Furthermore, the materials and methods used for dielectric metasurface fabrication make them CMOS-compatible. Dielectric metasurfaces are typically made of high refractive index materials such as silicon, germanium, or tellurium on IR transparent substrates such as Si, SiO_2, MgF_2 or CaF_2 by utilizing electron beam lithography fabrication in research and prototyping. The dielectric metasurfaces investigated in this work are made of Si on SiO_2 or MgF_2 substrates of different thicknesses.

2.9 Applications of CO_2 sensors incorporating dielectric metasurfaces

Photosynthesis can be monitored by measuring the uptake of CO_2 in plant leaves, since CO_2 is consumed through the stomatal pores and metabolized in the leaves during this process via the following chemical reaction:

$$6CO_2 + 6H_2O + light \rightarrow C_6H_{12}O_6 + 6O_2 \quad (10)$$

If CO_2 is readily available for photosynthesis and is not the limiting reagent in the process, CO_2 consumption rate depends on the availability of the other reactants – water and light. Hence, if water or light is insufficient for the maximum photosynthetic capacity, the CO_2 consumption will be relatively lower compared to the CO_2 consumption at maximum rate of photosynthesis. This can help in tracking plant health and optimizing water supply. Photosynthesis also exhibits

an activity dependence on leaf (and plant) age[45]. The link between CO_2 concentration and plant infection probability and severity has been studied[46].

The uptake of CO_2 during optimal photosynthetic conditions varies depending on the plant type, however, mesophytes in temperate zones consume approximately 1-4 µmol CO_2 per hour, per cm^2 [47]. For the small changes to be detected in measuring plant CO_2 consumption in research or on the field, the sensor must have very high sensitivity and accuracy, and preferably low detection limit, all features of a CO_2 sensor based on metasurface sensing technology.

If CO_2 is insufficient, it facilitates the reverse reaction of photosynthesis – respiration, therefore plants start losing water through transpiration from the stomatal pores[48]. The water vapour concentration change in air around the plant leaf could also be an indicator of photosynthetic rate and insufficient CO_2 availability, suggesting water vapor monitoring in addition to CO_2 levels to ensure optimal photosynthetic rate. As water also has mid-IR active vibrational modes, a metasurface gas sensor can be tuned to also detect changes in water vapor concentration. It is even possible to develop a multi-resonant metasurface geometry to combine detection of multiple gases on one sensing surface.

Another use of such sensors is capnography. Capnography is the measurement of the end tidal CO_2 or in other words – CO_2 in exhaled breath. As the CO_2 levels in exhaled breath and the CO_2 levels in the bloodstream are directly correlated, by measuring the CO_2 levels in human breath the CO_2 levels in the blood can be deduced and thus conclusions can be made regarding the health condition of a patient.

Furthermore, CO_2 in its liquid or solid form is increasingly used in refrigeration for cold rooms and walk-in freezers due to lower global warming potential of CO_2 as compared to other gases in use. However, if concentrations of CO_2 in air become too high (over 5000 ppm), it can become dangerous for humans. Thus, if leaks occur in refrigeration systems and they go undetected, it can seriously harm the people in the near vicinity[49]. CO_2 refrigeration systems are often run under high pressure, therefore, quick leak detection is important, as the gas leak rate is very high and quickly raises the surrounding CO_2 concentration. When concentrations rise above 5000 ppm, a potential gas leak must be investigated. This can be done by a hand-held CO_2 detector. For CO_2 monitoring near refrigeration systems, the detector requirements include good resolution and accuracy at 0.5% and 1.0% set points and high enough upper detection limit to detect truly dangerous CO_2 concentrations (3%-4%). Since CO_2 detection is a point detection, it means that concentrations can be higher elsewhere in the room. Therefore, very fast response times to scan the room for places of potentially dangerous CO_2 concentrations would be desirable.

3 Experimental Part

Three different metasurface designs were examined for their application in CO_2 gas sensing. Designs were based on the following works:

- Ali, M. O. *et al. JOSA A* **35**, 119–124 (2018)[50] – denoted "cylindrical" and "cylindroid" structures for simplicity.
- Tittl, A. *et al. Science* **360**, 1105 (2018)[40] – denoted "slanted ellipse" structure for simplicity.
- Wu, C. *et al. Nat. Commun.* **5**, 3892 (2014)[44] – denoted "Pi" structure for simplicity.

A scaling factor S was applied to the metasurface geometries, as shown in table 2, to match their resonant frequencies to the CO_2 molecular vibrations at 4.3 µm.

All numerical simulations were carried out using COMSOL Multiphysics 5.2 software (RF Module). The Frequency Domain finite element method was employed to model the resonant responses of the metasurfaces to incident electromagnetic radiation.

The metasurface responses to incident IR light were probed in reflection and transmission mode, using single and double port boundary conditions, respectively. The incident plane wave propagating in the z-direction in most cases was polarized in the x-direction. However, the cylindrical and cylindroid structures were irradiated by unpolarized light as for the cylindrical structure being symmetrical there is no difference in the x and y directions, and for the cylindroid structure the resonant response arising from the x and y polarizations can be clearly distinguished (see fig. A1). Periodic boundary conditions in the x- and y-directions were used to mimic infinite array of metasurface unit cells in two directions. A perfectly matched layer (PML) was used on the boundary opposite to excitation port in order to absorb all radiation passing through the structure to avoid unwanted back-reflections.

The parameters for the simulations are compiled in table 2 and depicted in figures 4-6. To conserve the computing power, some thickness parameters (fig. 5) were reduced to a computable size without affecting the qualitative outcome of the simulation, such as the thickness of air, the thickness of the Si handle, and the thickness of the MgF_2 substrate.

The spectral dependence on the angle α and β (fig. 6) of the incoming light was measured.

To calculate the field enhancement ($|E|^2/|E_0|^2$), a shell was constructed around the nanoresonators at a distance of 10 nm and an average value across the surface was calculated. Field enhancement spatial distribution for the Pi structure was calculated.

To get an understanding of the electric field intensity within and surrounding the metasurfaces the field profiles ($|E|^2$) were plotted at the resonant frequencies.

Table 2. Simulation parameters for all structures studied in this work. h_PML is the thickness of the perfectly matched layer; h_Cu is the thickness of the copper backreflector; h_Si is the reduced handle thickness of the silicon on insulator (SOI) substrate; h_SiO_2 and h_MgF_2 are the reduced thicknesses of the SiO_2 and MgF_2 substrate layers respectively; h_MS is the height of the metasurface (thickness of the nanoresonators); h_air – reduced thickness of air; S – scaling factor of dimensions. The simulation thickness parameters and the unit cell geometrical parameters are explained in figures 4 and 5, respectively.

Parameter	Cylinder and cylindroid unit cells	Slanted ellipse unit cell	Pi unit cell
Px, µm	2.75*S	3.92*S	2.40*S
Py, µm	2.75*S	2.26*S	2.40*S
h_PML, µm	1.00	2.50	3.00
h_Cu, µm	1.00	N/A	N/A
h_Si, µm	N/A	N/A	3.00
h_SiO_2, µm	1.90	N/A	1.60
h_MgF_2, µm	N/A	2.50	N/A
h_MS, µm	0.80	0.70	1.20
h_air, µm	3.00	3.00	3.00
a, µm	0.60*S (cylinder) or 0.54*S (cylindroid)	0.96*S	N/A
b, µm	0.60*S	1.96*S	N/A
θ, °	N/A	20	N/A
w, µm	N/A	N/A	0.500*S
d, µm	N/A	N/A	0.700*S
g, µm	N/A	N/A	0.200*S
L, µm	N/A	N/A	2.000*S
S	N/A (1.13)	0.73	0.985

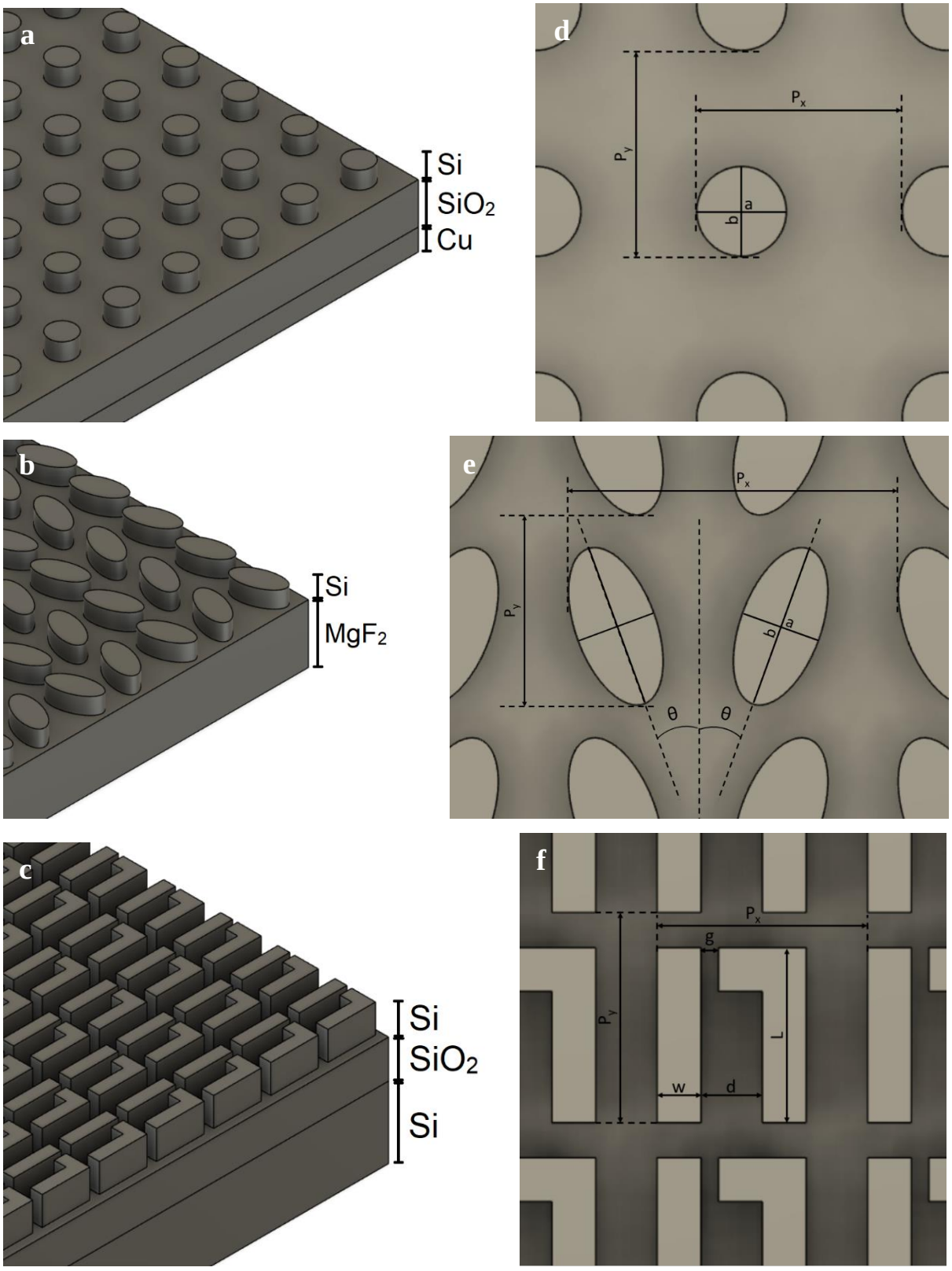

Figure 4. (a-c) Metasurface layer schematic representation for cylindrical/cylindroid, slanted ellipse, and Pi unit cell metasurfaces, respectively; (d-f) surface geometrical parameter representation for cylindrical/cylindroid, slanted ellipse, and Pi unit cell metasurfaces, respectively.

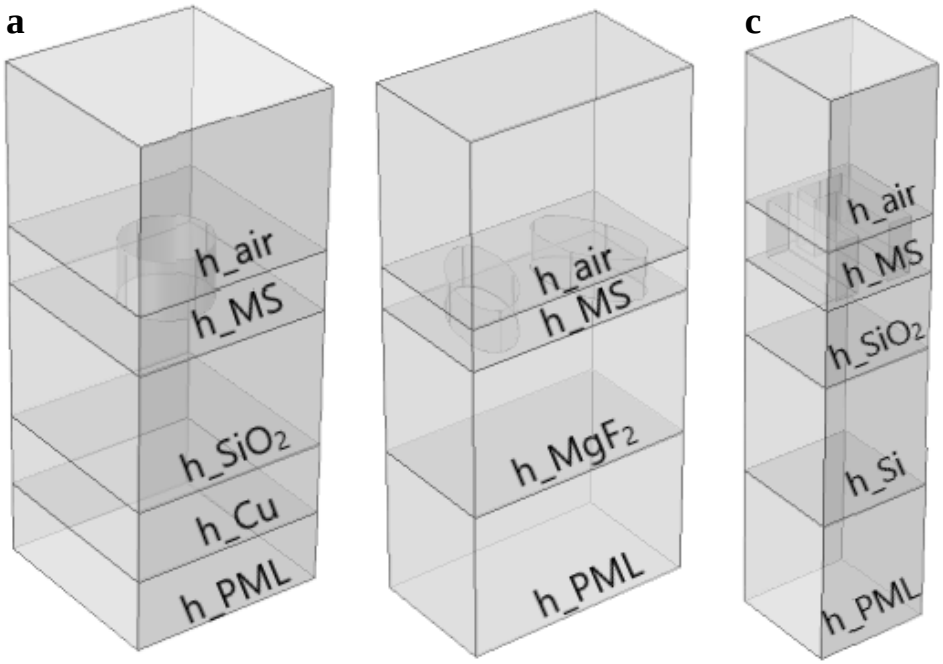

Figure 5. thickness parameter spatial representation in simulations of the (a) cylindrical/cylindroid, (b) the slanted ellipse, and (c) the Pi structure.

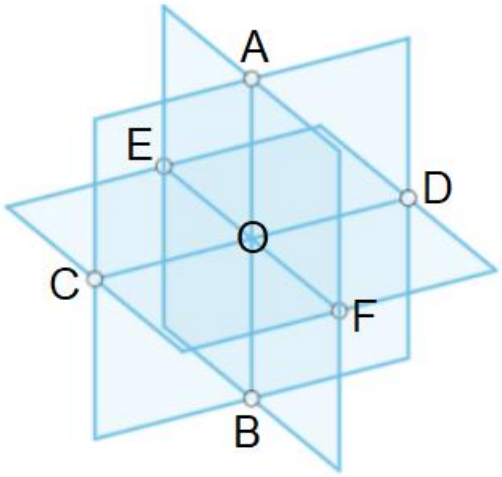

Figure 6. Representation of planes and axes and definition of incident angle. AB is the z axis, CD is the x axis, and EF is the y axis; O is the origin point (0;0;0); ∠AOC = α, ∠AOF=β; AO – normal incidence.

4 Results and Discussion

For applications in CO_2 gas sensing a new concept of an optical sensor incorporating metasurfaces was explored. Four different geometries of unit cells were studied and characterized for their suitability in such applications.

4.1 Cylindrical and cylindroid unit cell

The simplest unit cell designs based on research by M. O. Ali *et al.* – a cylindrical and an elliptical cylinder (cylindroid) shape – was probed only in reflection mode (fig. 7-9, A1-A3) as a copper backreflector, being opaque in the mid-IR range prevented the examination of the metasurface in transmission mode. When considering the experimental setup for measurements in reflection mode the light source and the detector must be on the same side of the metasurface, making it inconvenient to conduct measurements at normal incidence. Even if semi-transparent mirrors were used allowing for measurements with incident light at exactly 90° to the metasurface, positioning the light source with zero deviation from normal incidence could still prove challenging. Furthermore, the mirrors would cause quite significant (approx. 50%) signal intensity losses. When considering the light source, if normal incidence is to be achieved, it must have no beam divergence and thus a laser source or a collimated beam would be preferred. However, lasers are expensive and beam collimation introduces an additional element to the system, adding to the overall complexity. And even with such light sources the configurational issues are still present. Due to the mentioned challenges in attaining normal incidence, the spectral response to varying angles of incident light was examined for all metasurfaces explored in this work.

The reflection spectrum of the cylindrical unit cell metasurface (fig. 7) exhibits a sharp dip in reflectance at around 4.02 μm wavelength and some additional spectral features which appear as a result of more complex interactions between electric and magnetic dipoles of the Si nanoresonator and the metal backreflector, however, these spectral features would not pose an issue in sensing applications. The sharp dip at 4.02 μm, which is the resonant feature of interest, shows a very high quality factor of Q = 1664, which is attractive for the intended application as described in the previous sections.

The cylindroid unit cell reflection spectrum (fig. 8) shows two dips in reflectance, which is expected due to the asymmetry of the unit cell in the x and y directions. The separation of the spectral features accounting for x and y-polarized incident light is shown in figure A1.

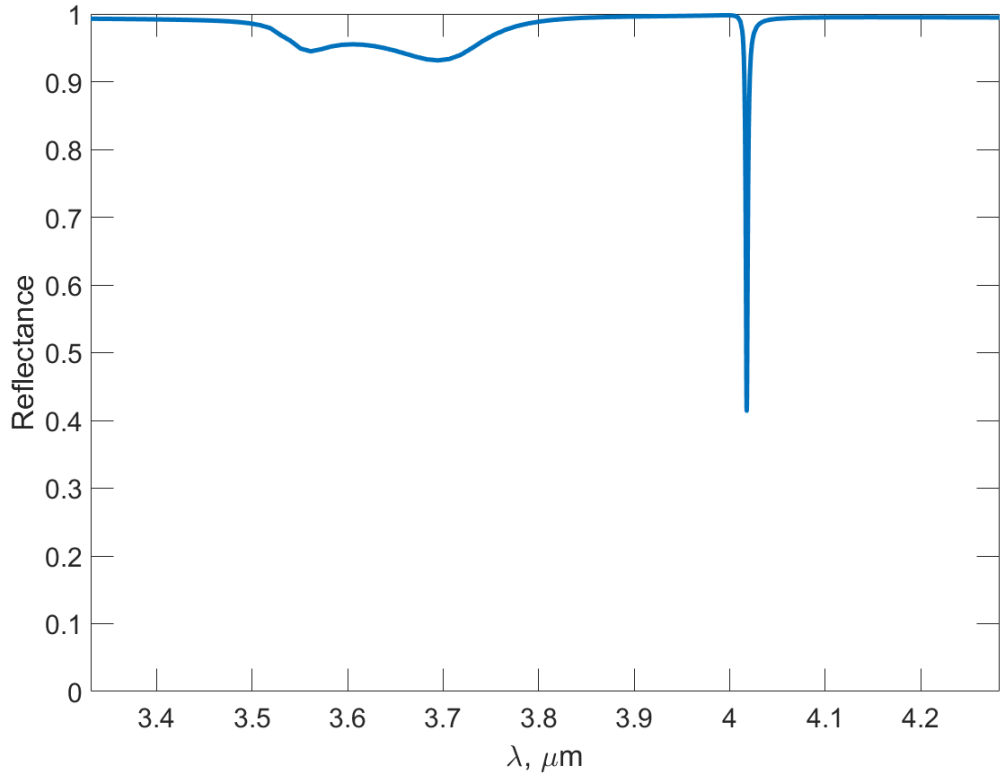

Figure 7. Unpolarized light reflectance spectrum of the cylindrical unit cell metasurface.

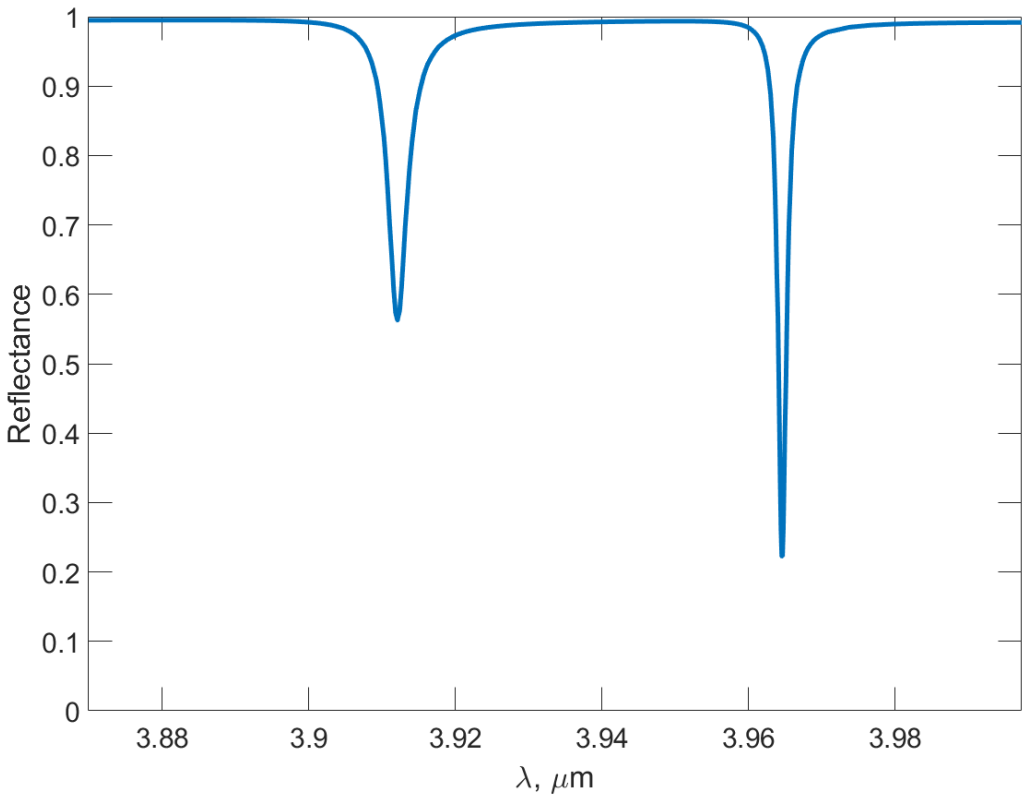

Figure 8. Unpolarized light reflectance spectrum of the cylindroid unit cell metasurface.

The dependence of the cylindrical unit cell metasurface reflectance spectrum on the angle of incident light was studied (fig. 9). As the cylindrical unit cell is symmetrical, the spectral response with varying the angle α and β should be the same. The dependence of the cylindroid unit cell metasurface reflectance spectrum on the angle α and β of the incident light is shown in appendix figures A2 and A3, respectively.

With increasing the angle of the incident light for the cylindrical unit cell metasurface, very little deviation from the normal incidence peak position at approximately 4.02 μm can be observed. A more detailed angle dependence plot around this resonance feature is depicted in figure A4. Appearance of more resonance features around the reflectance dip at 4.02 μm can be seen with increasing the angle of incident light above 0°. The minimal shift in peak position with increasing the incident light angle suggests that this type of unit cell could be used reliably in CO_2 sensors.

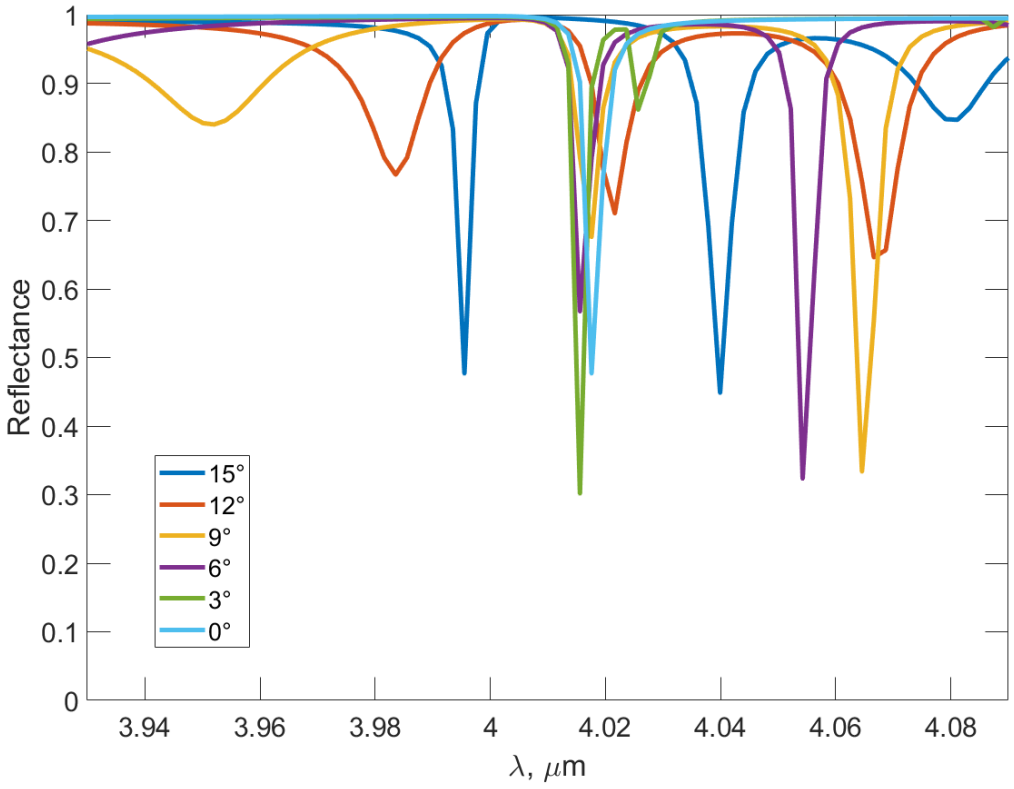

Figure 9. Unpolarized light reflectance spectrum dependence on the angle α of the incident light for the cylindrical unit cell metasurface.

When examining the electric field profiles at the resonance wavelength for the cylindrical and cylindroid structures (fig. 10-12) it can be seen that the electric field is not confined only inside the unit cell material, some field enhancement can also be seen surrounding the structures.

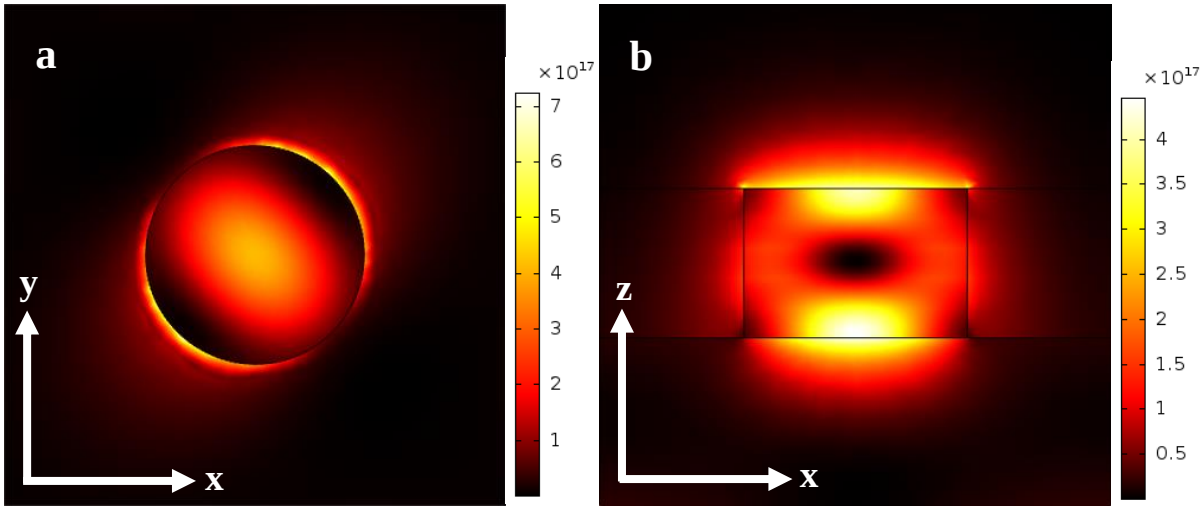

Figure 10. Electric field intensity in the xy plane on top of the metasurface (a) and in the xz plane at Py/2 position of the unit cell (b) at the resonant wavelength (4.02 μm) for the cylindrical unit cell metasurface.

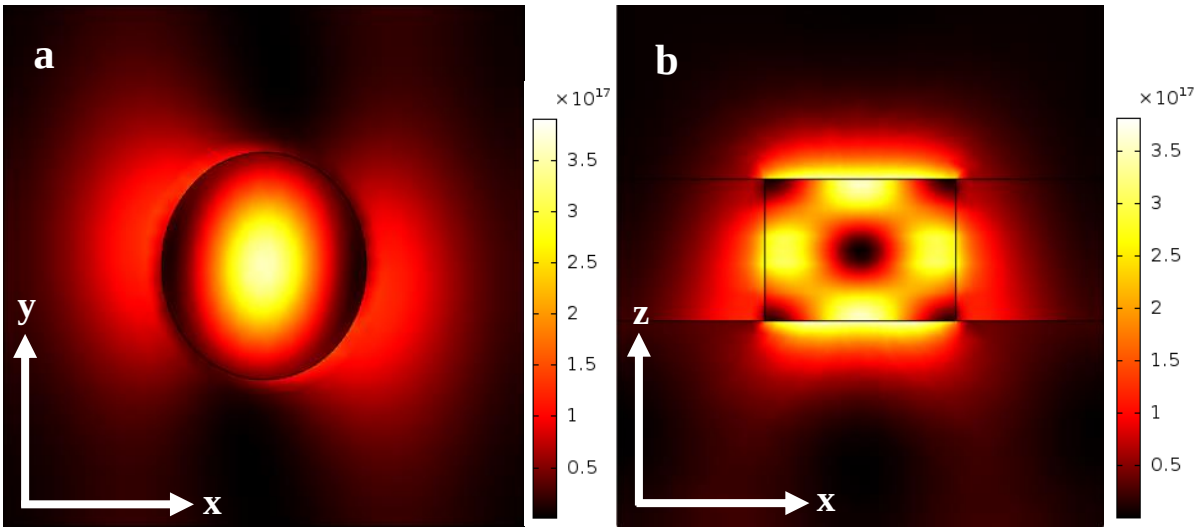

Figure 11. Electric field intensity in the xy plane on top of the metasurface (a) and in the xz plane at position Py/2 of the unit cell (b) at the y-resonant wavelength (3.912 μm) for the cylindroid unit cell metasurface.

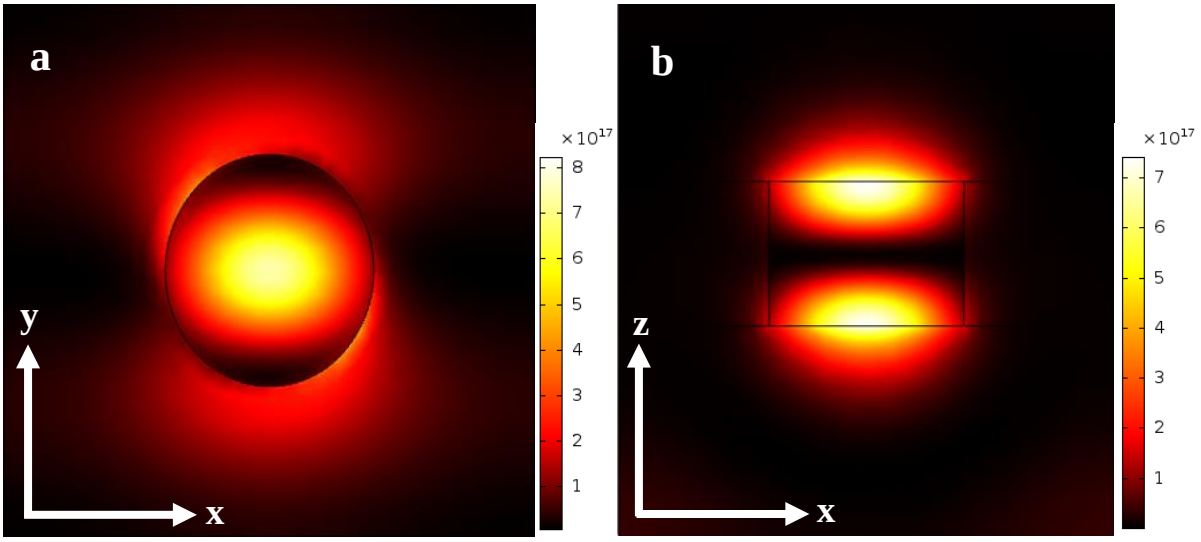

Figure 12. Electric field intensity in the xy plane on top of the metasurface (a) and in the xz plane at position Py/2 of the unit cell (b) at the x-resonant wavelength (3.965 μm) for the cylindroid unit cell metasurface.

Even though the characteristics of the metasurface comprised of the cylindrical and cylindroid unit cell, such as low incident light angle dependence, simple structure, and high Q factors make them appear appealing in applications for gas sensing, the possibility to take measurements only in reflection mode pose configurational challenges as described above.

Furthermore, as application in CO_2 gas sensing demands for the resonant features of the metasurfaces to coincide with the CO_2 molecular vibrations at around 4.3 μm, a scaling factor S = 1.13 was applied to the dimensions of the unit cell (table 2) to appropriately tweak the resonant response (fig. A5). Even though the spectral feature moved to the desired frequency region, its intensity greatly weakened, rendering it inadequate for applications in CO_2 gas sensing. Further adjustments could be made to the metasurface geometry to regain the resonant response strength, however, the limited possibilities in carrying out experiments with this type of metasurface do not justify the effort. Hence, other structures were also explored for said application.

4.2 Two slanted ellipse unit cell

The metasurface comprised of the slanted ellipses gave promising results when probed in reflection and transmission mode, exhibiting practically perfect reflection (fig. 13).

The scaling of the metasurface from the research article[40] was tuned so that the resonance peak would coincide with the molecular vibration frequency of CO_2 molecules.

The quality factor of the resonance feature when observed either in reflection or transmission mode was high (Q = 135) and the spectrum was clean without any additional resonance features in the background making it highly selective if irradiated with a broadband light.

When the incident light angle dependence was studied (fig. 14 (α) and A6 (β)), however, the peak position shifted a lot (up to 0.04 μm) even at low variations in the incident light angle (0°-4°). As CO_2 sensing depends on the modulations in resonant responses, including shift in peak position, having it shift considerably just due to angle deviations is problematic. Furthermore, as normal incidence is extremely difficult to achieve due to configurational challenges of optical systems as described in the previous section, some angle divergence from normal incidence will always be present. Thus, the spectral angle dependence is an important characteristic to be assessed when evaluating any metasurface for sensing applications.

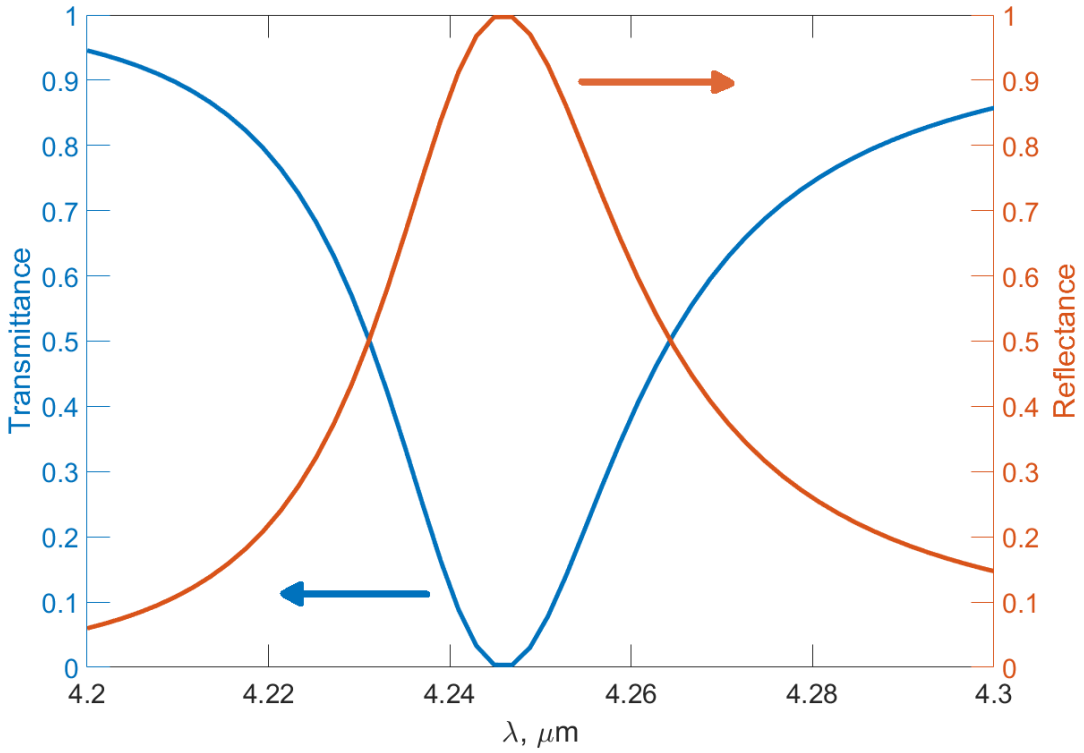

Figure 13. x-polarized incident light reflectance and x-polarized transmittance spectrum of the slanted ellipse unit cell metasurface.

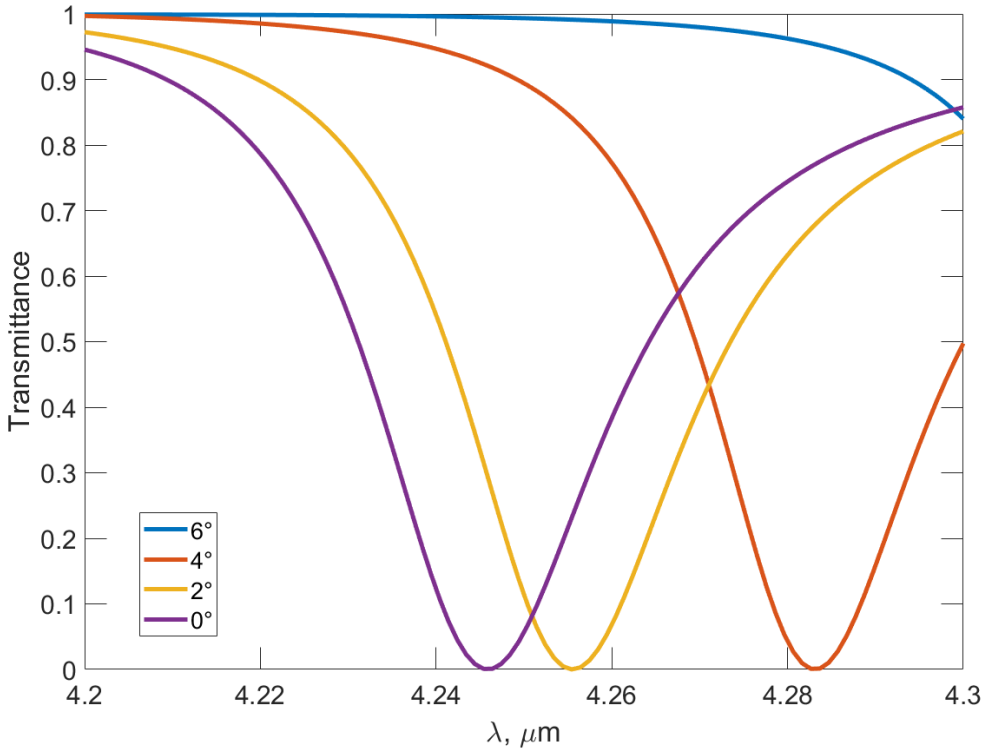

Figure 14. x-polarized incident light x-polarized transmittance spectrum dependence on the angle α of the incident light for the slanted ellipse unit cell metasurface.

When looking at the electric field profiles at the resonance for this structure (fig. 15) it can be seen that the fields are localized strongly outside of the metasurface, which is a very attractive property for a metasurface used in sensing as it improves the light-matter interactions. However, the major drawback of the pronounced shift in peak position even at low incident light angle deviations complicates the use of such a metasurface in a CO_2 gas sensor whose accuracy and sensitivity depend on the modulations in the resonance feature in response to CO_2 concentration changes. Thus, another unit cell geometry was explored incorporating two parallel Si resonators with a symmetry-breaking rod for possible application in CO_2 gas sensing.

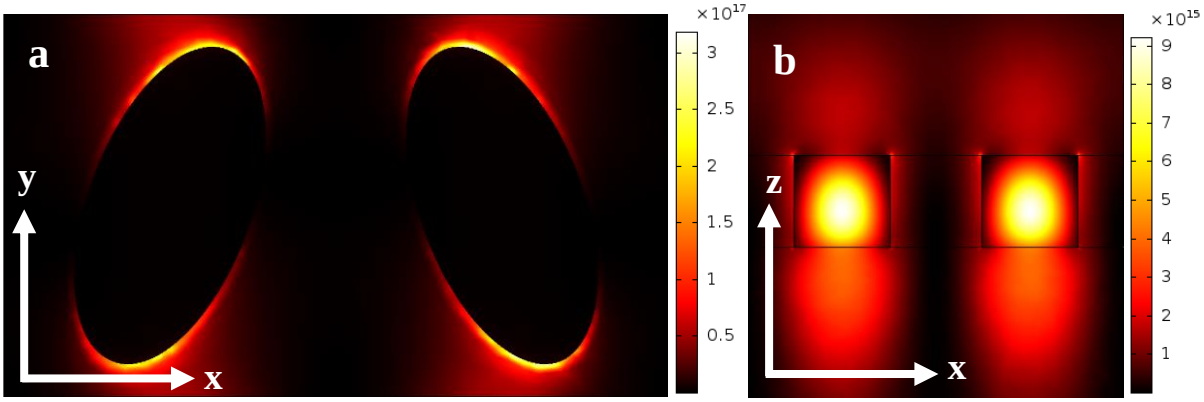

Figure 15. Electric field intensity in the xy plane on top of the metasurface (a) and in the xz plane at Py/2 position of the unit cell (b) at the resonant wavelength (4.245 µm) for the slanted ellipse unit cell metasurface.

4.3 Pi structure unit cell

The metasurface based on research by C. Wu *et al.* (the Pi structure metasurface) has shown the most promising results and potential for application in CO_2 gas sensing. When probing the metasurface in transmission mode, a transmission maximum with high Q factor (Q = 131) was observed (fig. 16, blue line). The metasurface geometry was scaled so that the peak position would coincide with the CO_2 molecular vibrations at around 4.3 µm.

When investigating the field enhancement at a distance of 10 nm from the structure in the region near the resonance peak, an increase in the field enhancement value of over 35 can be seen (fig. 16, red line). As mentioned before, high field enhancement means increased interactions between the metasurface resonant modes and CO_2 molecular vibrations, and, together with high-Q spectral features, it enables high-sensitivity detection.

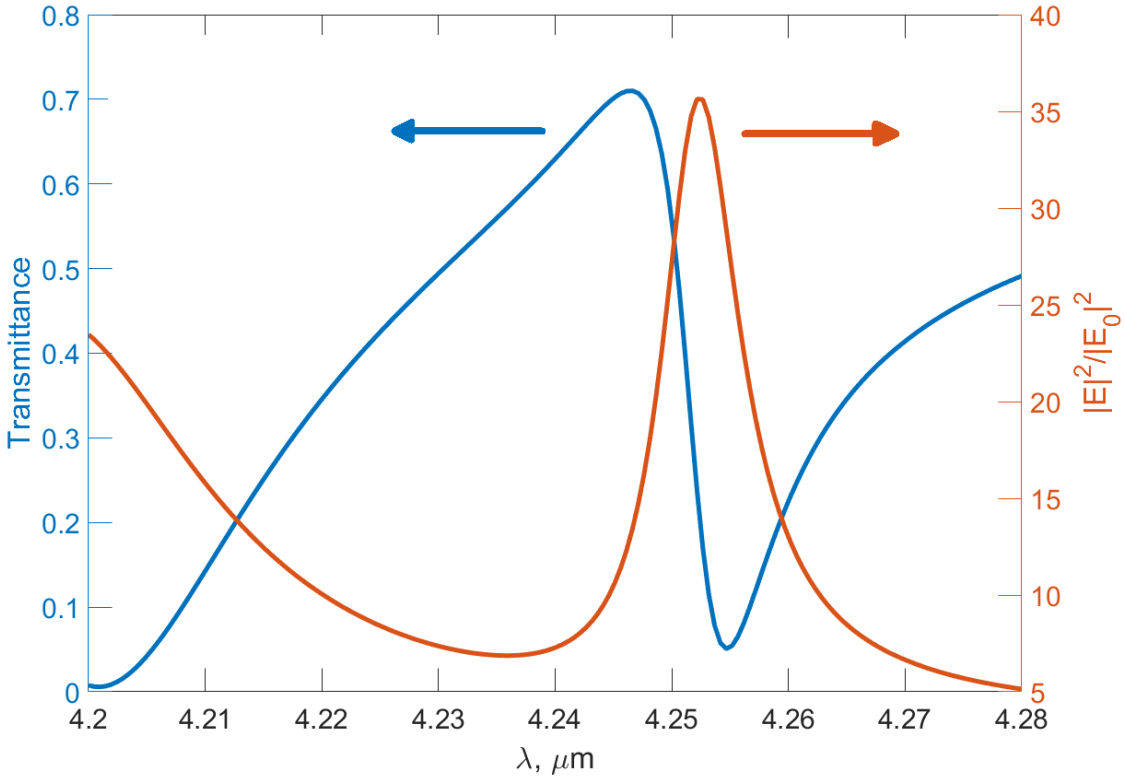

Figure 16. x-polarized transmittance of x-polarized light and field enhancement ($|E|^2/|E_0|^2$) surface average of the shell 10 nm from the unit cell surface for the Pi unit cell metasurface.

Incident light angle α dependence investigation (fig. 17) showed only slight shift in the peak position with increasing incident light angle as compared to the slanted ellipse unit cell structure. Incident light angle β dependence is depicted in figure A7.

The very slight shift in the transmission peak position with increased incident light angle means that the spectral response of the Pi unit cell metasurface is more resistant to configurational errors when setting up optical systems and the divergence of light rays of a non-laser light source which may introduce incident light angle deviation.

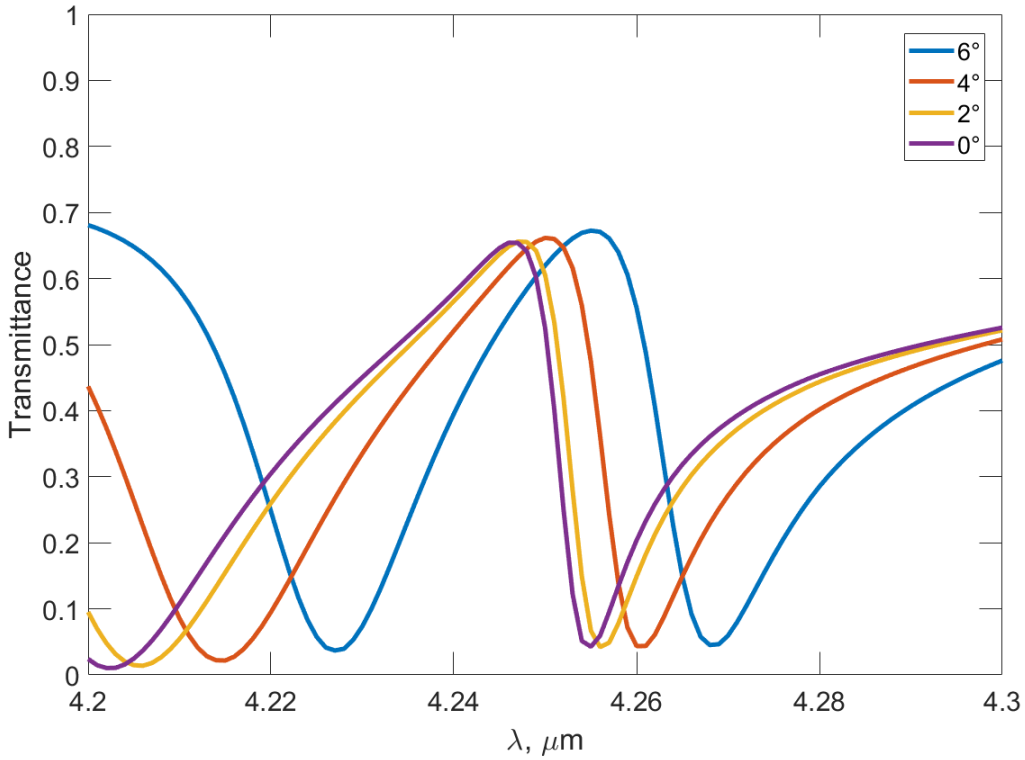

Figure 17. x-polarized light transmittance spectrum dependence on the angle α of the incident x-polarized light for the Pi unit cell metasurface.

Investigation of the electric field profiles (fig. 18) confirmed that most of the field is confined within the metasurface structures, namely within the material, however, some field enhancement extending beyond the surface of the structure can also be observed, which can be utilized in improved sensing of changes in the surrounding environment.

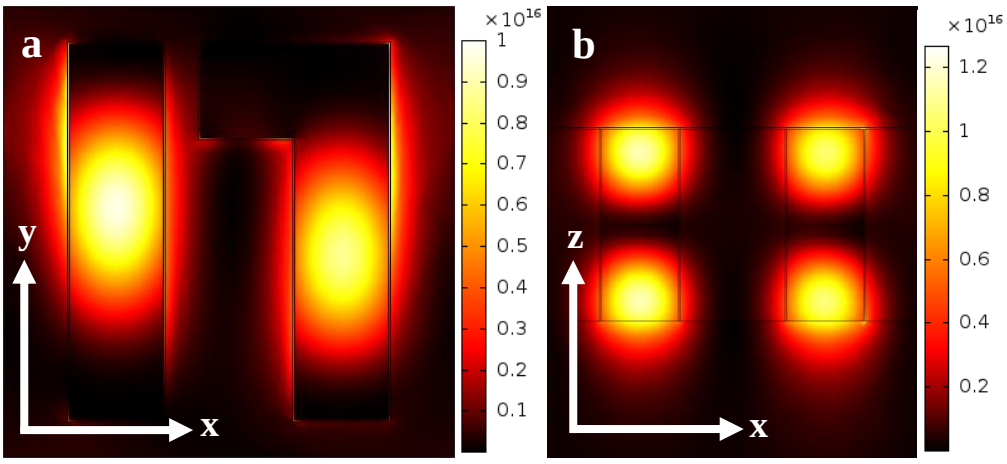

Figure 18. Electric field intensity in the xy plane on top of the metasurface (a) and in the xz plane at Py/2 position of the unit cell (b) at the resonant wavelength (4.248 μm) for the Pi unit cell metasurface.

The spatial distribution of the field enhancement is shown in figure 19 and it was evaluated as the average field enhancement across the xy plane at an increasing distance above the unit cell. As can be seen from the graph, the field enhancement drops quickly as the distance from the metasurface is increased. The field intensity profile in figure 18b shows the same trend that most field intensity is located within the material, and it quickly decreases as the distance from material is increased. If high field enhancement would extend to a far distance from the metasurface it would increase the more efficient light-matter interaction cross-section. Nevertheless, having field enhancement confined to the vicinity of the metasurface allows for reduction in the length of the gas chamber, which is governed by how strong the field enhancement near the metasurface is – the higher the field enhancement near the metasurface, the more the gas chamber length can be reduced.

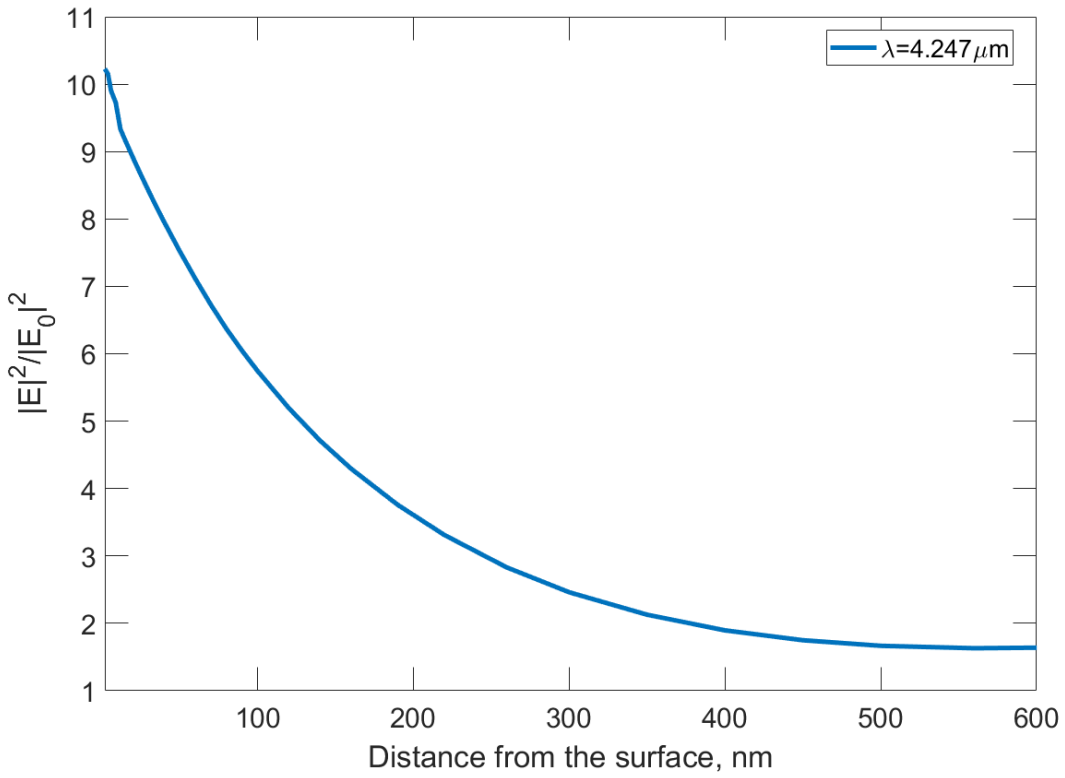

Figure 19. Field enhancement spatial distribution graph at the resonant wavelength (4.247 μm) for the Pi unit cell metasurface.

4.4 Outlook

The next steps in implementing the metasurface technology in CO_2 sensing involve conducting experimental studies of the gas concentration measurements utilizing metasurfaces to validate

the theoretical research presented in this work. For this purpose, substrates have been obtained to be used in metasurface fabrication by EBL.

Once experimental validation is complete, and metasurfaces can be successfully incorporated in CO_2 gas sensors, the technology can be taken to market and nanoimprint lithography can be utilized to fabricate metasurfaces in larger quantities. Manufacturing metasurfaces on such a large scale would be required as the demand for the technology increases. A superficial market analysis has revealed that the CO_2 sensor market is indeed a growing sector, accounting for 20% revenue share of the overall gas sensor market (valued at 1.5 billion in 2019) and is expected to experience a 4% growth until 2026[1]. The promising metrics are a great motivator in pursuing the research and carrying it all the way to production.

The main application areas where the metasurface-incorporated CO_2 sensor could emerge as a strong competitor are photosynthesis monitoring, capnography (exhaled CO_2 monitoring), research, and any other field that would benefit from a small, convenient, and cost-efficient CO_2 detection device with high sensitivity and selectivity, fast response time, and convenient use for personal and industry applications.

5 Conclusions

Dielectric metasurfaces studied in this work show promising features applicable in CO_2 gas sensing, such as high-Q resonances and high field enhancement near the sensing surface.

The metasurface based on cylindrical unit cell structure showed low angle dependence, however, the possibility to carry out experiments only in reflectance mode hinders its application in CO_2 gas sensing.

The metasurface based on the slanted ellipse unit cell showed a high-Q resonance peak and field enhancement outside of the nanoresonators. However, it also exhibited very high dependence on incident light angle, making it unattractive for sensing applications due to large modulation introduced in the spectrum with even moderate incident beam divergence, despite having no analyte present. Beam divergence would essentially cause smearing out of the sharp spectral feature and effective lowering of the Q factor. This issue suggests the use of a laser source or a beam collimator, and both of these options have their drawbacks as discussed before.

Based on the simulations carried out in this work the most promising metasurface for application in CO_2 gas sensing proved to be the one consisting of the Pi structure unit cell. The Pi unit cell metasurface exhibited high-Q (Q = 131) resonance peak at around the wavelength of CO_2 molecular absorption (4.3 μm), field enhancement of over 35 at 4.252 μm 10 nm from the unit cell surface, and electric field intensity enhancement reaching beyond the surface of the unit cell structure.

Incorporating metasurfaces in high precision CO_2 sensors could enable a sensitive, selective, small, convenient, fast responding, and cost-efficient device, as compared to devices currently on the market. The photosynthesis monitoring devices currently on the market exhibit satisfactory accuracy (down to 1% at 200 ppm[51]) and yield reliable results, however, the drawbacks are undeniable. Firstly, the large device size and weight (as much as 44 cm in length and 1.5 kg in weight[52] and larger) makes it difficult for the user to carry out prolonged measurements on a portable device without resting. Second, the response time of the devices is largely limited by diffusion of CO_2 into the sample chamber (min 35 s[52]) even if the measurement recording can be done faster. And finally, the price of the available plant monitoring devices is typically extremely high[53]. These disadvantages could potentially be eradicated by incorporating metasurfaces in CO_2 sensing.

Publications and Conferences

The 9th NRW Nano Conference in Münster, Germany (held online), April 21-23, 2021, participation with a poster presentation.

Acknowledgements

I would like to express my gratitude to my supervisor Glen for the effort put into teaching me the basics of metasurface physics, broadening my knowledge in the complicated field of physics in general, helping me to gain participation in the 9th NRW Nano Conference in Münster, Germany, and being a great motivator and an inspiration to continue pursuing a career in science.

I am grateful to my teachers during the past two years who were supportive in our learning and eager to help us achieve our academic goals.

I would also like to thank my family and friends for being understanding during the thesis writing period and helping me feel supported when times were tough.

References

1. Gas Sensors Market Size & Share | Global Forecasts 2026. *Global Market Insights, Inc.* https://www.gminsights.com/industry-analysis/gas-sensors-market-size.
2. Chen, J., Gu, J., Zhang, R., Mao, Y. & Tian, S. Freshness Evaluation of Three Kinds of Meats Based on the Electronic Nose. *Sensors* **19**, 605 (2019).
3. Liu, L., Li, X., Li, Z. & Shi, Y. Application of Electronic Nose in Detection of Fresh Vegetables Freezing Time Considering Odor Identification Technology. *Chem. Eng. Trans.* **68**, 265–270 (2018).
4. Manzoli, A. *et al.* Volatile compounds monitoring as indicative of female cattle fertile period using electronic nose. *Sens. Actuators B Chem.* **282**, 609–616 (2019).
5. Harrou, F., Dairi, A., Sun, Y. & Kadri, F. Detecting Abnormal Ozone Measurements With a Deep Learning-Based Strategy. *IEEE Sens. J.* **18**, 7222–7232 (2018).
6. Raja Kumar, J. R., Pandey, R. K. & Sarkar, B. K. Pollutant Gases Detection using the Machine learning on Benchmark Research Datasets. *Procedia Comput. Sci.* **152**, 360–366 (2019).
7. Nasiri, N. & Clarke, C. Nanostructured Gas Sensors for Medical and Health Applications: Low to High Dimensional Materials. *Biosensors* **9**, 43 (2019).
8. Bochenkov, V. & Sergeev, G. Sensitivity, selectivity, and stability of gas-sensitive metal-oxide nanostructures. in *Metal Oxide Nanostruct. Appl.* vol. 3 31–52 (2010).
9. Sarf, F. Metal Oxide Gas Sensors by Nanostructures. *Gas Sens.* (2019) doi:10.5772/intechopen.88858.
10. Parrino, F. & Palmisano, L. *Titanium Dioxide (TiO2) and Its Applications*. (Elsevier, 2020).
11. Dey, A. Semiconductor metal oxide gas sensors: A review. *Mater. Sci. Eng. B* **229**, 206–217 (2018).

12. Hahn, S. H. *et al.* CO sensing with SnO2 thick film sensors: role of oxygen and water vapour. *Thin Solid Films* **436**, 17–24 (2003).
13. Fine, G. F., Cavanagh, L. M., Afonja, A. & Binions, R. Metal Oxide Semi-Conductor Gas Sensors in Environmental Monitoring. *Sensors* **10**, 5469–5502 (2010).
14. Karakaya, D., Ulucan, O. & Turkan, M. Electronic Nose and Its Applications: A Survey. *Int. J. Autom. Comput.* **17**, 179–209 (2020).
15. Cavicchi, R. E. Calorimetric Sensors. 287–320 (2011).
16. Park, N.-H., Akamatsu, T., Itoh, T., Izu, N. & Shin, W. Calorimetric Thermoelectric Gas Sensor for the Detection of Hydrogen, Methane and Mixed Gases. *Sensors* **14**, 8350–8362 (2014).
17. Ishihara, T. & Matsubara, S. Capacitive Type Gas Sensors. *J. Electroceramics* **2**, 215–228 (1998).
18. Keimel, A. Comparison of Low-Cost CO2 Non-Dispersive Infrared (NDIR) Sensors for Ambient Greenhouse Gas Monitoring. *UVM Honors Coll. Sr. Theses* (2019).
19. Hodgkinson, J., Smith, R., Ho, W. O., Saffell, J. R. & Tatam, R. P. Non-dispersive infra-red (NDIR) measurement of carbon dioxide at 4.2μm in a compact and optically efficient sensor. *Sens. Actuators B Chem.* **186**, 580–588 (2013).
20. Carbon dioxide. *Wikipedia* (2021).
21. Alexander Berk. Can You Use CO2 for TIG Welding? *Welding Mastermind* https://weldingmastermind.com/can-you-use-co2-for-tig-welding/.
22. Earth's CO2 Home Page. *CO2.Earth* https://www.co2.earth/.
23. Carbon Dioxide. *Wisconsin Department of Health Services* https://www.dhs.wisconsin.gov/chemical/carbondioxide.htm (2018).
24. Jaggard, K. W., Qi, A. & Ober, E. S. Possible changes to arable crop yields by 2050. *Philos. Trans. R. Soc. B Biol. Sci.* **365**, 2835–2851 (2010).

25. Kovenock, M. & Swann, A. L. S. Leaf Trait Acclimation Amplifies Simulated Climate Warming in Response to Elevated Carbon Dioxide. *Glob. Biogeochem. Cycles* **32**, 1437–1448 (2018).
26. Zosel, J., Oelßner, W., Decker, M., Gerlach, G. & Guth, U. The measurement of dissolved and gaseous carbon dioxide concentration. *Meas. Sci. Technol.* **22**, 072001 (2011).
27. Dinh, T.-V., Choi, I.-Y., Son, Y.-S. & Kim, J.-C. A review on non-dispersive infrared gas sensors: Improvement of sensor detection limit and interference correction. *Sens. Actuators B Chem.* **231**, 529–538 (2016).
28. Vibrational Modes of Carbon Dioxide. https://www.chem.purdue.edu/jmol/vibs/co2.html.
29. Popa, D. & Udrea, F. Towards Integrated Mid-Infrared Gas Sensors. *Sensors* **19**, 2076 (2019).
30. Infrared Spectroscopy. *Chemistry LibreTexts* https://chem.libretexts.org/Bookshelves/Physical_and_Theoretical_Chemistry_Textbook_Maps/Supplemental_Modules_(Physical_and_Theoretical_Chemistry)/Spectroscopy/Vibrational_Spectroscopy/Infrared_Spectroscopy/Infrared_Spectroscopy (2013).
31. Trivedi, R., Rai, N. & Bharadwaj, K. Metamaterial: Materials with Exceptional Properties. *Int. J. Eng. Res. Technol.* **2**, (2018).
32. Alitalo, P. & Tretyakov, S. Electromagnetic cloaking with metamaterials. *Mater. Today* **12**, 22–29 (2009).
33. Tang, Y. *et al.* Hybrid acoustic metamaterial as super absorber for broadband low-frequency sound. *Sci. Rep.* **7**, 43340 (2017).
34. Sajuyigbe, A. Electromagnetic Metamaterials for Antenna Applications. (2010).
35. Quevedo-Teruel, O. *et al.* Roadmap on metasurfaces. *J. Opt.* **21**, 073002 (2019).
36. Yan, Z. *et al.* Perfect Absorption and Refractive-Index Sensing by Metasurfaces Composed of Cross-Shaped Hole Arrays in Metal Substrate. *Nanomaterials* **11**, 63 (2021).

37. Wang, Y., Ali, Md. A., Chow, E. K. C., Dong, L. & Lu, M. An optofluidic metasurface for lateral flow-through detection of breast cancer biomarker. *Biosens. Bioelectron.* **107**, 224–229 (2018).

38. Ray, D. *et al.* Hybrid Metal-Dielectric Metasurfaces for Refractive Index Sensing. *Nano Lett.* **20**, 8752–8759 (2020).

39. Hu, J., Lang, T., Wu, M., Zhao, R. & Chen, J. Refractive index sensing using all-dielectric metasurface with analogue of electromagnetically induced transparency. in *2017 16th International Conference on Optical Communications and Networks (ICOCN)* 1–3 (2017). doi:10.1109/ICOCN.2017.8121410.

40. Tittl, A. *et al.* Imaging-based molecular barcoding with pixelated dielectric metasurfaces. *Science* **360**, 1105 (2018).

41. Guo, Z. *et al.* Active-Tuning and Polarization-Independent Absorber and Sensor in the Infrared Region Based on the Phase Change Material of Ge 2 Sb 2 Te 5 (GST). *Sci. Rep.* **8**, 12433 (2018).

42. Joe, Y., Satanin, A. & Kim, C. S. Classical analogy of Fano resonances. *Phys Scr* **7463**, (2006).

43. Zhang, J., Liu, W., Zhu, Z., Yuan, X. & Qin, S. Strong field enhancement and light-matter interactions with all-dielectric metamaterials based on split bar resonators. *Opt. Express* **22**, 30889 (2014).

44. Wu, C. *et al.* Spectrally selective chiral silicon metasurfaces based on infrared Fano resonances. *Nat. Commun.* **5**, 3892 (2014).

45. Bielczynski, L. W., Łącki, M. K., Hoefnagels, I., Gambin, A. & Croce, R. Leaf and Plant Age Affects Photosynthetic Performance and Photoprotective Capacity. *Plant Physiol.* **175**, 1634–1648 (2017).

46. Gullino, M. L., Pugliese, M., Gilardi, G. & Garibaldi, A. Effect of increased CO2 and temperature on plant diseases: a critical appraisal of results obtained in studies carried out under controlled environment facilities. *J. Plant Pathol.* **100**, 371–389 (2018).
47. Verduin, J. A Table of Photosynthetic Rates Under Optimal, Near-Natural Conditions. *Am. J. Bot.* **40**, 675–679 (1953).
48. Hille, K. Rising Carbon Dioxide Levels Will Help and Hurt Crops. *NASA* http://www.nasa.gov/feature/goddard/2016/nasa-study-rising-carbon-dioxide-levels-will-help-and-hurt-crops (2016).
49. CO2 Gas Detection - Calibration Technologies. https://www.ctiengineering.com/articles/co2-gas-detection/.
50. Ali, M. O., Tait, N. & Gupta, S. High-Q all-dielectric thermal emitters for mid-infrared gas-sensing applications. *JOSA A* **35**, 119–124 (2018).
51. LI-COR Biosciences - Impacting Lives Through Science. https://www.licor.com/env/products/photosynthesis/LI-6800/.
52. CI-340 Handheld Photosynthesis System | Tools for Applied Plant Science | cid-inc.com. https://www.cid-inc.com/plant-science-tools/photosynthesis-measurement/ci-340-handheld-photosynthesis-system/.
53. Hand-held Photosynthesis Systems. *ResearchGate* https://www.researchgate.net/post/Hand-held_Photosynthesis_Systems.

Appendix

Appendix 1

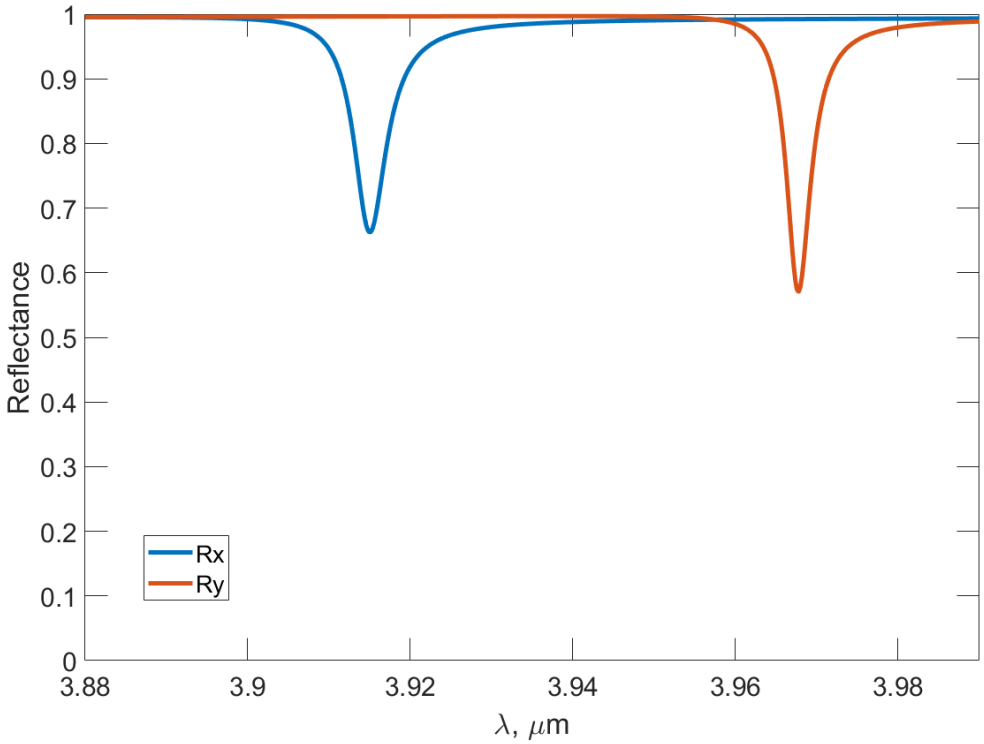

Figure A1. x-polarized (Rx) and y-polarized (Ry) light reflectance spectrum of the cylindroid unit cell metasurface.

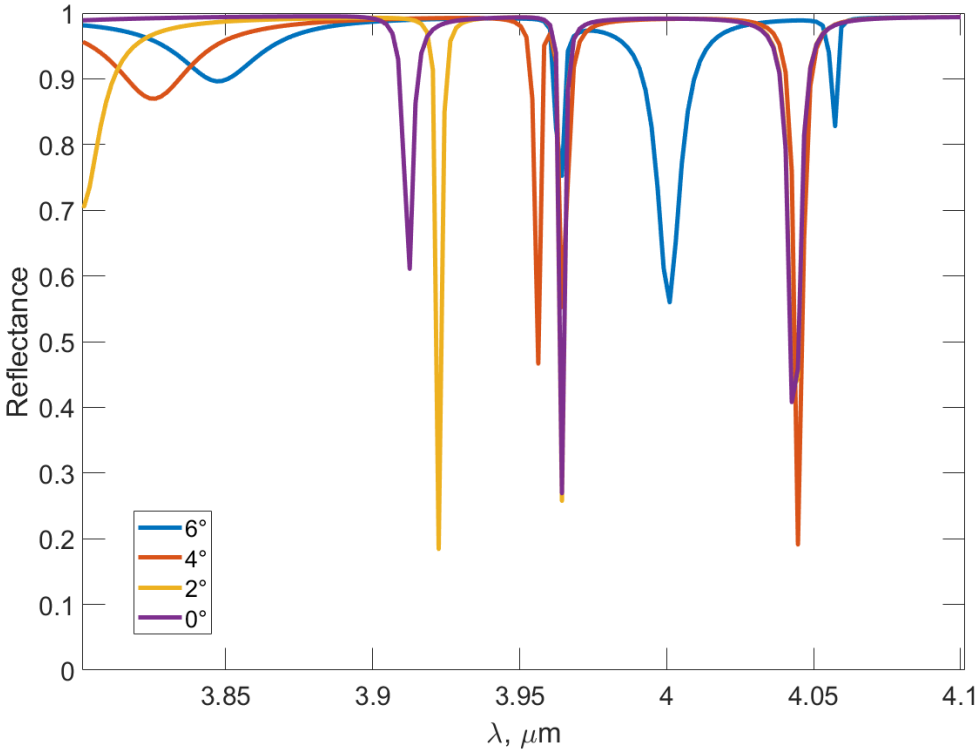

Figure A2. Unpolarized light reflectance spectrum dependence on the angle α of the incident light for the cylindroid unit cell metasurface.

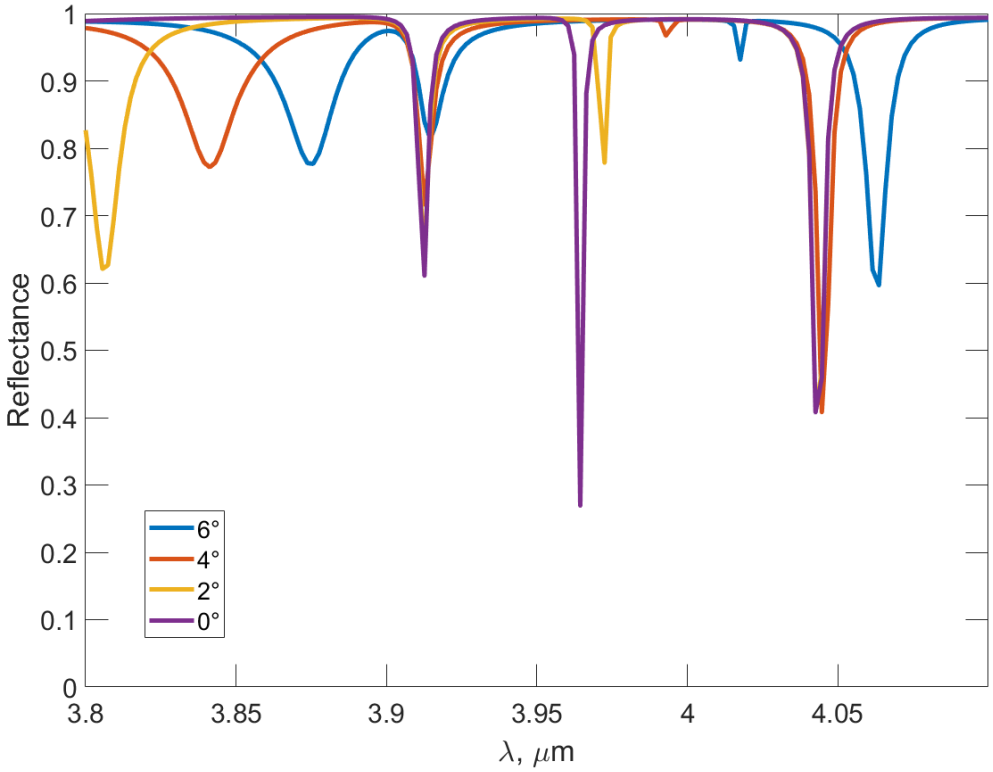

Figure A3. Unpolarized light reflectance spectrum dependence on the angle β of the incident light for the cylindroid unit cell metasurface.

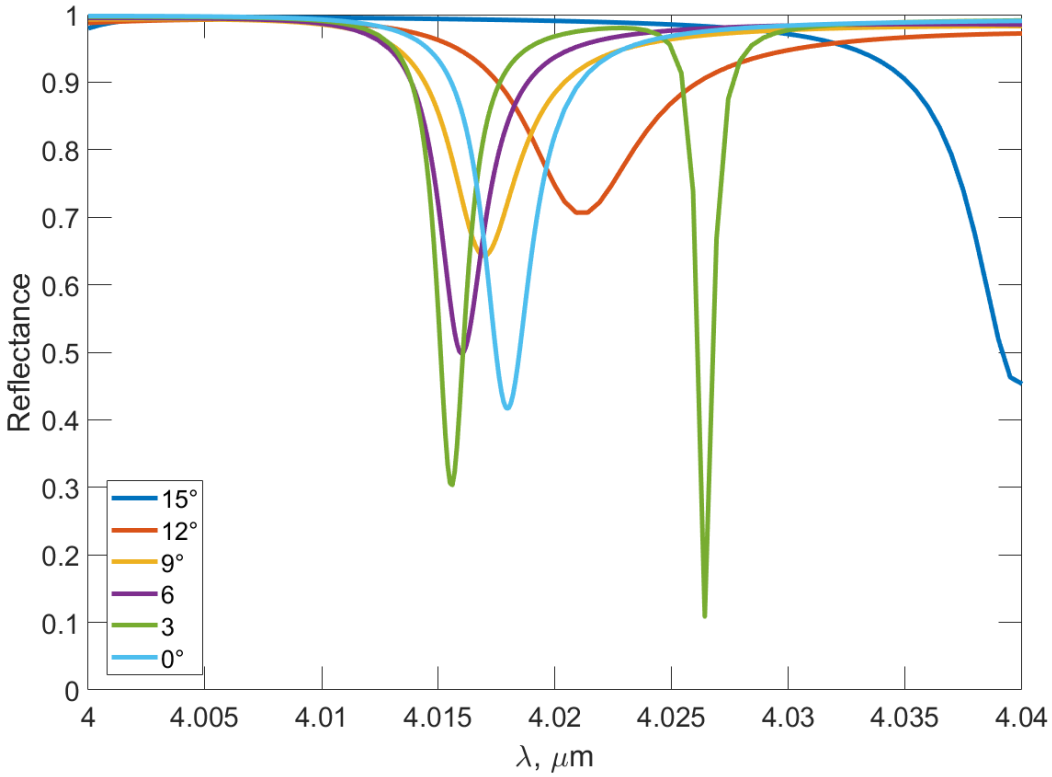

Figure A4. Unpolarized light reflectance spectrum dependence on the angle α of the incident light for the cylindrical unit cell metasurface, detailed.

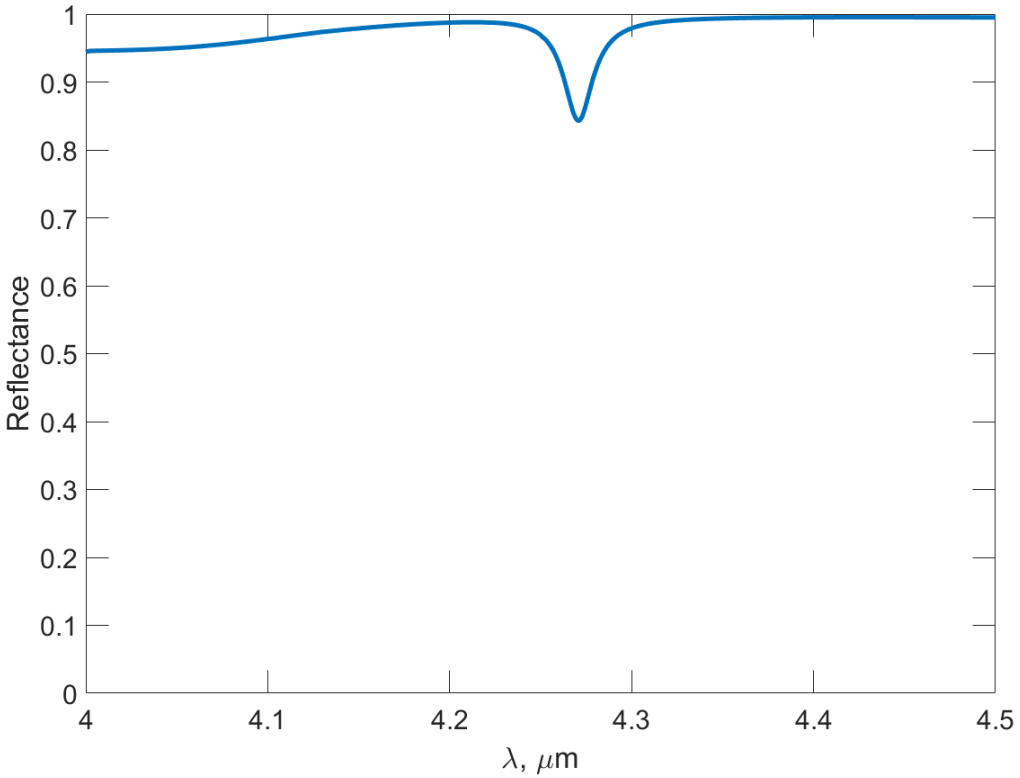

Figure A5. Unpolarized light reflectance spectrum of the scaled, but not optimized cylindrical unit cell metasurface.

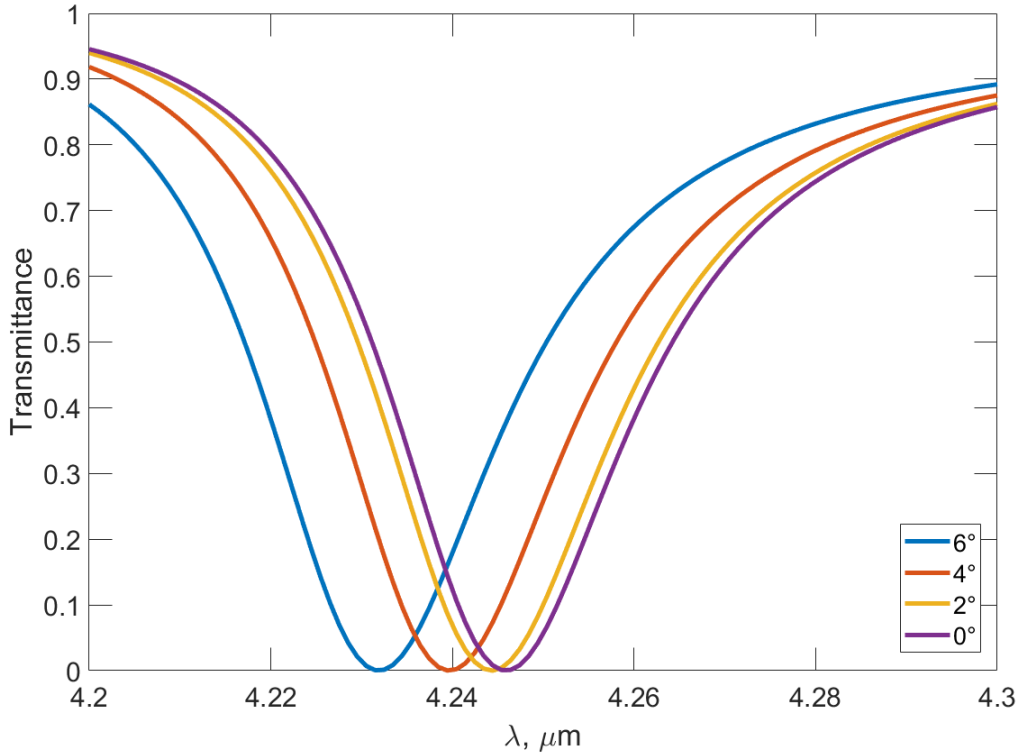

Figure A6. x-polarized transmittance spectrum dependence on the angle β of the x-polarized incident light for the slanted ellipse unit cell metasurface.

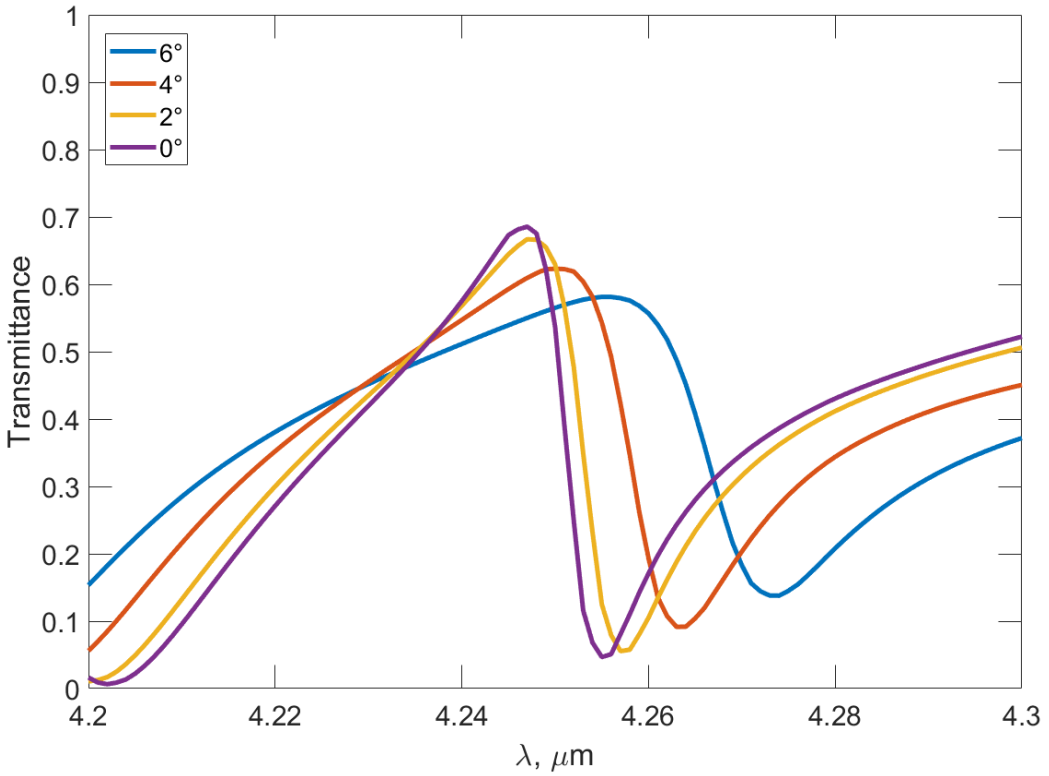

Figure A7. x-polarized light transmittance spectrum dependence on the angle β of the incident x-polarized light for the Pi unit cell metasurface.

Appendix 8

Non-exclusive licence to reproduce thesis and make thesis public

I, _____Liga Britala_____,

(*author's name*)

1. herewith grant the University of Tartu a free permit (non-exclusive licence) to

reproduce, for the purpose of preservation, including for adding to the DSpace digital archives until the expiry of the term of copyright,

_____"Dielectric metasurfaces for CO_2 gas sensing"_____

_____,

(*title of thesis*)

supervised by _____Glen Kelp_____.

(*supervisor's name*)

2. I grant the University of Tartu a permit to make the work specified in p. 1 available to the public via the web environment of the University of Tartu, including via the DSpace digital archives, under the Creative Commons licence CC BY NC ND 3.0, which allows, by giving appropriate credit to the author, to reproduce, distribute the work and communicate it to the public, and prohibits the creation of derivative works and any commercial use of the work until the expiry of the term of copyright.

3. I am aware of the fact that the author retains the rights specified in p. 1 and 2.

4. I certify that granting the non-exclusive licence does not infringe other persons' intellectual property rights or rights arising from the personal data protection legislation.

Liga Britala

04/06/2021